Structure and Evolution of Winter Cyclones in the Central United States and Their Effects on the Distribution of Precipitation. Part I: A Synoptic-Scale Rainband Associated with a Dryline and Lee Trough

JONATHAN E. MARTIN, JOHN D. LOCATELLI, PETER V. HOBBS, PENG-YUN WANG, AND JEFFREY A. CASTLE

Department of Atmospheric Sciences, University of Washington, Seattle, Washington

(Manuscript received 21 March 1994, in final form 14 July 1994)

ABSTRACT

A convective rainband, which was approximately 1500 km in length and affected large areas of the central United States for about 16 h, developed within an evolving winter cyclone. The rainband, which will be referred to as the *pre-drytrough rainband,* formed approximately 400 km ahead of a developing dryline and lee trough (*drytrough,* for short) that created an elevated, sloping layer of convective instability. The presence of a deep pool of high-potential-temperature air in the middle troposphere over the south-central United States, advected there from the elevated terrain to the southwest (i.e., an elevated mixed layer), produced a region of warm-air advection downstream of the high terrain. This enhanced the lifting associated with a migrating short wave aloft and generated the pre-drytrough rainband.

In previous studies the dryline, the lee trough, the elevated mixed layer, and the low-level jet in the central United States have generally been viewed as isolated features. Here the authors present a more integrated view, compelled by their common dependence on the interactions of synoptic-scale disturbances with topography.

Mesoscale structures and precipitation distributions similar to those documented in this paper are common in winter cyclones in the central United States and they are responsible for much of the severe weather associated with these systems.

1. Introduction

Extratropical cyclones are generally accompanied by the development of precipitation features that are organized on various scales by a variety of physical processes. Over the past quarter of a century, considerable effort has been devoted to documenting and explaining the location and intensity of organized mesoscale precipitation features in extratropical cyclones (e.g., Browning et al. 1973; Harrold 1973; Hobbs 1978; Bennetts and Hoskins 1979; Hobbs et al. 1980; Matejka et al. 1980; Martin et al. 1992; Locatelli et al. 1994, 1995). These studies have encompassed oceanic cyclones over the eastern Atlantic Ocean (Browning and Monk 1982), the eastern Pacific Ocean (Hobbs 1978), and the western Atlantic Ocean (Shapiro and Keyser 1990), as well as continental cyclones undergoing modifications by maritime influences on the east coast of the United States (Locatelli et al. 1989; Sienkiewicz et al. 1989). By comparison, relatively little attention has been paid to extratropical cyclones deep within the interiors of continents. This paper is the first in a series describing a number of synoptic and mesoscale structures associated with winter cyclones in the central United States and their effects on precipitation. In this series of papers we will use detailed datasets collected during the Storm Operational and Research Meteorology-Fronts Experiment Systems Test (STORM-FEST) field program, which took place in the central United States from 1 February to 15 March 1992. The focus of the present paper is the role of the Rockies and the Mexican Plateau in the formation of a synoptic-scale rainband that occurred within a major continental cyclone that affected the central United States from 8 to 10 March 1992 (hereafter referred to as the "Super Tuesday" storm).

The development of winter cyclones in the central United States is greatly affected by the geography of the region. The influences of the subtropical Gulf of Mexico to the south, the Rocky Mountains to the west, and the frigid Canadian Arctic to the north combine to produce cyclonic disturbances that are often quite different in structure from that depicted in the classical Norwegian cyclone model (Bjerknes and Solberg 1922), which was based on observations of maritime cyclones as they made landfall in western Europe. Of particular importance for precipitation in winter cyclones over the central United States are the interactions of synoptic-scale waves with the varied topography of the region. These interactions can produce *lee troughs* (Carlson 1961; Steenburgh and Mass 1994),

Corresponding author address: Peter V. Hobbs, Department of Atmospheric Sciences, University of Washington, Seattle, Washington 98195.

the *dryline* (Fujita 1958; McGuire 1960; Schaefer 1974, 1986), the *low-level jet* (Bonner 1968; Djuric and Damiani 1980; Djuric and Ladwig 1983), and the *elevated mixed layer* (Carlson et al. 1983; Benjamin and Carlson 1986). These features have generally been viewed as isolated from each other. Yet, their common dependence on the interactions of synoptic-scale features with topography requires a more integrated view. This series of papers will lay the foundation for such a viewpoint.

In this paper we describe the development of a cyclone observed during intensive observing period (IOP) 17 of STORM-FEST. We will show that this cyclone was characterized by a nonclassical distribution of precipitation. Specifically, we will detail the structure and dynamics of a 1500-km-long rainband that formed approximately 400 km ahead of a surface pressure trough that had the characteristics of both a lee trough and a dryline, which we term a *drytrough.* The surface trough had a shallow vertical circulation, similar to a classical warm front. The rainband of interest, which we shall term the *pre-drytrough rainband,* developed at the leading edge of an isolated region of warm-air advection at middle levels that was located within a broad zone of convective instability created by the warm frontal–like circulation associated with the surface trough. Thus, the pre-drytrough rainband was a regional manifestation of the scale-interactive processes that play a crucial role in organizing and distributing precipitation in cyclonic storms.

In section 2 we give a brief review of the lee trough, the dryline, the low-level jet, and the elevated mixed layer. This will set the stage for our discussion of the development of the synoptic-scale structure of the Super Tuesday storm. In section 3 we describe numerical model simulations that were used to diagnose the structure and dynamics of this cyclone. In sections 4 and 5 we diagnose the pre-drytrough rainband in some detail and discuss mechanisms for its production. The evolution of the cyclone is discussed in section 6, and the paper concludes with a discussion (section 7) and conclusions (section 8).

2. Some important meteorological features associated with cyclones in the central United States

Before turning to the Super Tuesday storm, we review briefly the characteristics of several nonclassical meteorological structures that are often associated with cyclones in the central United States, and which were present in the Super Tuesday storm.

a. The lee trough

The lee trough is a surface pressure feature that forms in the lee of the Rocky Mountains. Lee troughs play a significant role in the generation of severe weather east of the Rockies (Gaza and Bosart 1985; Benjamin and Carlson 1986; Hobbs et al. 1990), they can contribute to the creation of nonclassical, warm occluded–like structures (Locatelli et al. 1989; Martin et al. 1990; Hobbs et al. 1990), and they aid the development of the dryline (Benjamin and Carlson 1986; Martin et al. 1990). Steenburgh and Mass (1994) have reviewed this feature and present evidence that the eastern portion of the lee trough has characteristics similar to a shallow warm front. This is because the lee trough is largely a hydrostatic reflection of a low-level, warm-air anomaly produced by subsidence in the lee of the Rockies. As a result, the axis of the lee trough often coincides with the axis of the warmest surface potential temperatures.

b. The dryline

The dryline is a horizontal discontinuity in moisture that is confined to the lowest 1–3 km above the earth's surface. It tends to form at the confluence of moist air flowing northward from the Gulf of Mexico and desiccated air descending, in southwesterly flow, from the elevated desert plateaus of Mexico and the southwestern United States. The moist air east of the dryline is capped by a pronounced temperature inversion located at the base of an air mass with thermodynamic characteristics similar to those of the dry air to the west of the dryline (Schaefer 1974). This inversion allows convective instability in the lowest levels of the atmosphere to increase with time by inhibiting the development of deep convection. The dryline is often the focus of deep convection (Rhea 1966) and exhibits a diurnal migration (eastward during the day, westward at night) during "fair weather" dryline episodes (Schaefer 1974). By "fair weather" drylines we mean those drylines that exist in synoptically quiescent conditions (i.e., with no systematic surface development). Schaefer (1986) noted that the dryline is "often associated with a pressure trough and/or wind shift line" but that "neither feature is necessary for dryline existence." Martin et al. (1990) suggested that drylines form as a result of the same processes that form lee troughs, hence our term *drytrough.*

c. The low-level jet

A ubiquitous feature of cyclones in the central United States is the low-level jet (Bonner 1968; Djuric and Ladwig 1983). This is a low-level wind speed maximum, confined in the vertical, that occurs east of a surface pressure trough in the south-central United States. The low-level jet (LLJ) almost always appears at the bottom of an inversion layer and contributes to the northward transport of water vapor and latent heat into developing cyclonic disturbances in the central United States. Djuric and Damiani (1980) present a conceptual model for the development of the LLJ that

suggests lee troughing is of fundamental importance for the production of low-level wind maxima. Palmen and Newton (1969) suggest that the LLJ is vertically isolated as a result of an anomalously warm layer above it, which assists in the creation of a northerly thermal wind above the level of the LLJ core. This warm air is responsible for the creation of the inversion that accompanies the LLJ.

d. The elevated mixed layer

The elevated mixed layer (EML) is a deep, well-mixed layer of air formed by diabatic heating over the elevated Mexican Plateau. Carlson et al. (1983) present a conceptual model for the EML. With the approach of a baroclinic wave from the west, this deep layer loses contact with the ground as it travels downstream over lower terrain, and it eventually overruns moist and potentially cooler air in the southcentral United States. The potentially cooler air is therefore capped by a restraining inversion formed by the vertical juxtaposition of the base of the elevated mixed layer and low-level isentropes. The presence of this restraining lid inhibits the development of convection over a large region, as discussed by Carlson and Ludlam (1968). The western boundary of the EML is often characterized by moderate baroclinicity at middle levels (Carlson et al. 1983), which can initiate frontogenetically driven, secondary circulations at the edge of the lid that assist the development of severe convection (Keyser and Carlson 1984).

3. Numerical model simulations

Whenever possible, observations were used to analyze the Super Tuesday storm. However, to supplement the observations, and to carry out detailed diagnoses of the pre-drytrough rainband and the storm system in which it formed, the National Center for Atmospheric Research (NCAR)–Pennsylvania State University Mesoscale Model (MM4 version 8) was used. This model has been described by Anthes and Warner (1978) and Anthes et al. (1987). The version we used includes a high-resolution PBL model, based on the work of Blackadar (1979) and Zhang and Anthes (1982), an explicit moisture scheme (i.e., prognostic equations for water vapor, cloud water, and rainwater), and the Grell (1993) convective parameterization scheme. The domain contains 61 × 61 grid points with a grid size of 45 km (centered at 37°N, 96°W for case A, and at 40°N, 96°W for case B). The model atmosphere is divided into 23 layers in the vertical from the surface to 50 mb and uses the sigma vertical coordinate system.

The model was initialized using the National Meteorological Center (NMC) gridded data as the "first guess" field, supplemented by NMC Northern Hemispheric operational surface and rawinsonde data, and snow cover and land-use data prepared and maintained by NCAR. The lateral boundary conditions were linearly interpolated in time using observational data at 12-h intervals.

Two 24-h numerical experiments were run: case A initialized at 0000 UTC 8 March 1992, and case B initialized at 1200 UTC 8 March 1992. The need for case A became apparent upon initiation of trajectory analysis, when it was found necessary to trace air parcels back to 0000 UTC 8 March. Both simulations were very accurate for the first 12 h, but case A did not capture all of the mesoscale details of the storm structure after 12 h and was therefore used primarily for trajectory analysis. It is important to note that, despite their overall accuracy, at 45-km horizontal resolution neither case A nor case B predicted the occurrence of the 1500-km-long pre-drytrough rainband. This was a result of the model's inability, at this resolution, to accurately depict the thermodynamic conditions associated with the rainband. The synoptic-scale vertical motion associated with the rainband was accurately reproduced by the model simulations.

4. Life history of the pre-drytrough rainband

Figure 1 shows the National Weather Service (NWS) radar summary for 1535 UTC 8 March 1992. In addition to somewhat banded precipitation across

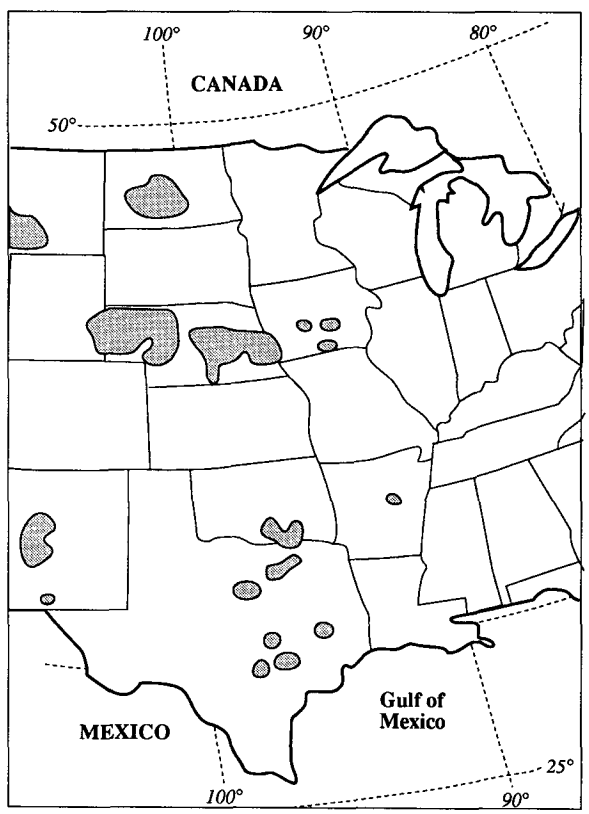

FIG. 1. National Weather Service (NWS) radar summary chart for 1535 UTC 8 March 1992. Regions of radar echo are shaded.

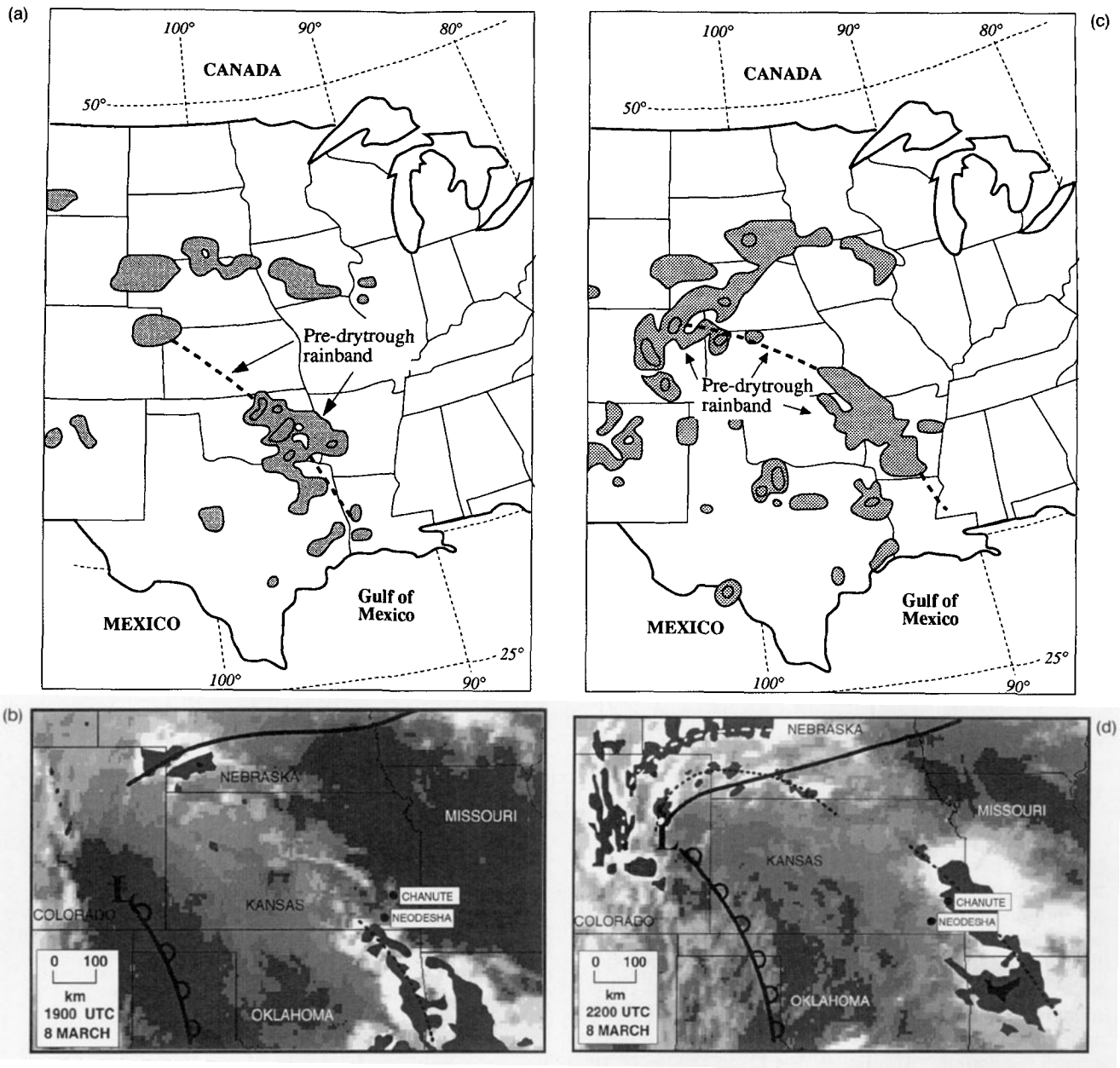

FIG. 2. (a) National Weather Service (NWS) radar summary chart for 1835 UTC 8 March 1992. Regions of radar echo are shaded. (b) Composite IR satellite image and NWS digitized radar data for 1900 UTC 8 March 1992 over the STORM-FEST intensive observing network. Radar echo shading is black for most intense reflectivities, and the heaviest shade of gray for less intense reflectivities, the lighter shades of gray are from the satellite imagery with white indicating the coldest cloud tops. Positions of Chanute, Kansas, surface observing station and Neodesha, Kansas, wind profiler station are indicated. The heavy solid line in Nebraska shows the position of the arctic front at the surface. The "L" is the position of the surface low pressure center, the scalloped line the position of the drytrough, and the dotted line shows the location of the pre-drytrough rainband. (c) National Weather Service (NWS) radar summary chart for 2135 UTC 8 March 1992. Regions of radar echo are shaded. (d) As for (b) but for 2200 UTC 8 March 1992. The dash–dot white line is the more northern portion of pre-drytrough rainband.

Nebraska and southern Iowa, there is a collection of scattered convective cells located in eastern Texas and southern Oklahoma (roughly straddling 97°W).

Three hours later, at 1835 UTC, the previously unconnected, scattered cells had evolved into a banded structure that occupied most of eastern Oklahoma and stretched, discontinuously, to coastal Texas (Fig. 2a). We will refer to this banded precipitation feature as the *pre-drytrough rainband.* Figure 2b shows a composite of the NWS digitized radar data and the IR satellite

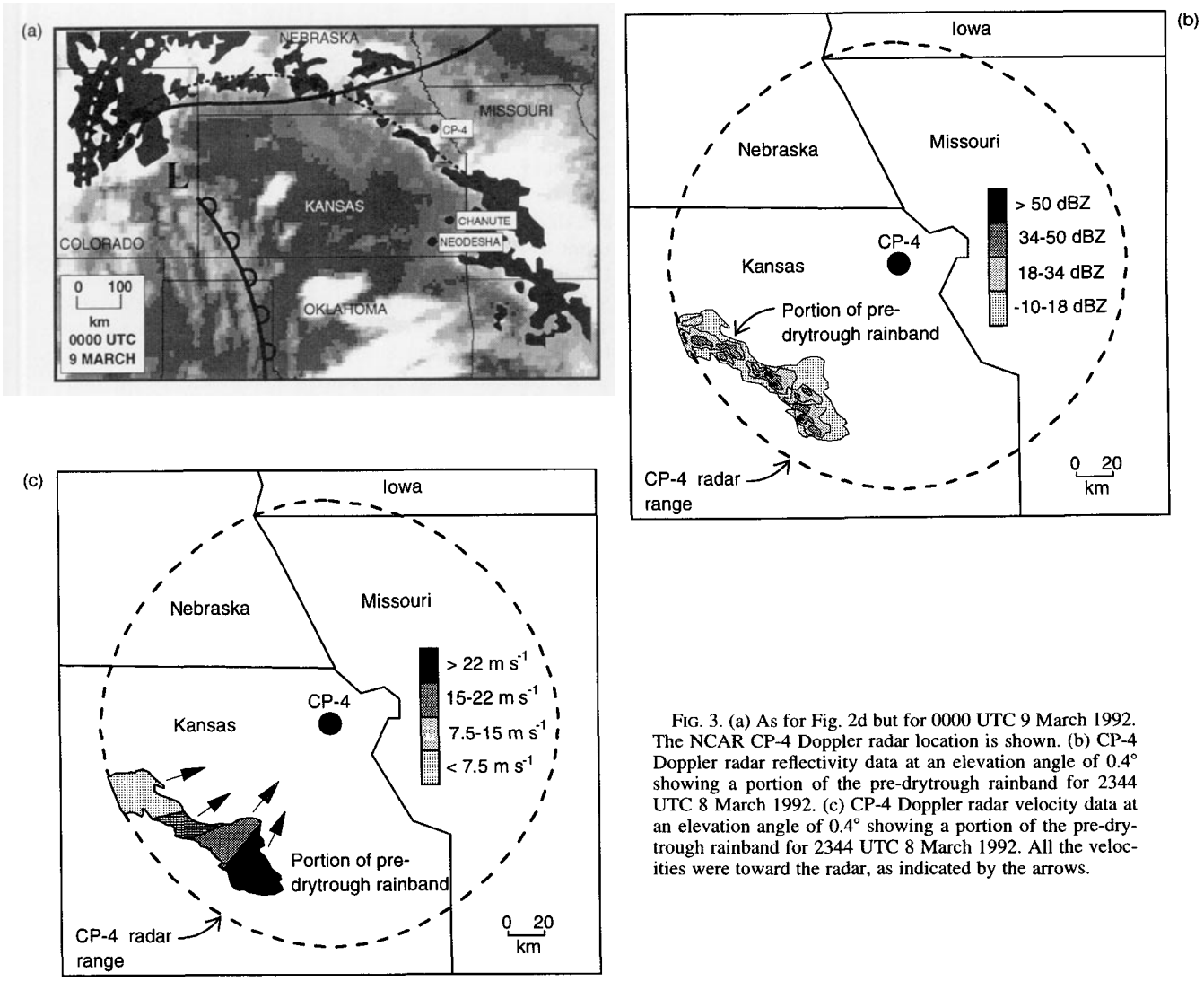

FIG. 3. (a) As for Fig. 2d but for 0000 UTC 9 March 1992. The NCAR CP-4 Doppler radar location is shown. (b) CP-4 Doppler radar reflectivity data at an elevation angle of 0.4° showing a portion of the pre-drytrough rainband for 2344 UTC 8 March 1992. (c) CP-4 Doppler radar velocity data at an elevation angle of 0.4° showing a portion of the pre-drytrough rainband for 2344 UTC 8 March 1992. All the velocities were toward the radar, as indicated by the arrows.

imagery at 1900 UTC 8 March within the intensive observational domain of STORM-FEST. This depiction shows that a nearly continuous band of high clouds connected the banded precipitation in Oklahoma to a region of thunderstorms along the borders of Nebraska, Kansas, and Colorado seen in Fig. 2a. By 2200 UTC 8 March, the rainband had become even better organized, as seen in both the NWS radar summary (Fig. 2c) and the composite satellite and radar data (Fig. 2d). The composite data suggests a double-banded structure in Colorado and the panhandle of Nebraska. By 2200 UTC 8 March much of the precipitation associated with the northern portion of the rainband was in the form of snow, as a shallow arctic front moved southward and the surface cyclone developed (Figs. 2b and 2d). The rainband shown in Fig. 2d was characterized by thundershowers and light to moderate rain along its length, with isolated embedded convective cells producing locally heavy rain, snow, and lightning. Composite data for 0000 UTC 9 March 1992 is shown in Fig. 3a. At this time, radar echoes stretched from extreme southeastern Arkansas (not shown), northwestward, into southern Nebraska toward Denver, Colorado. The NCAR CP-4 Doppler radar was located at Topeka, Kansas, during STORM-FEST and so Doppler reflectivity and velocity data are available for the analysis of portions of this rainband. These data vividly illustrate the convective nature of the pre-drytrough rainband, with reflectivities greater than 50 dBZ in the most intense convective cells (Fig. 3b). The corresponding Doppler velocity data (at approximately 850 mb) are shown in Fig. 3c. A low-level jet, from a direction of

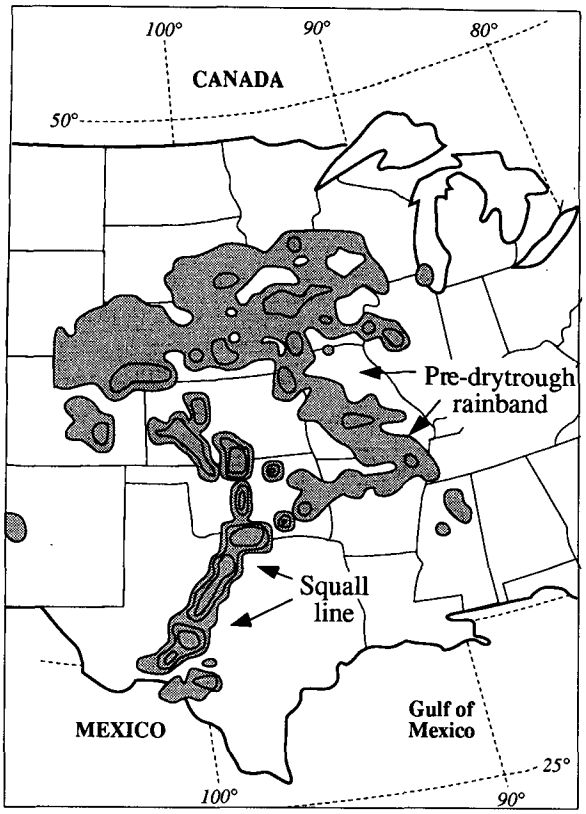

FIG. 4. National Weather Service (NWS) radar summary chart for 0235 UTC 9 March 1992. Regions of radar echo are shaded.

185°, was present across east-central Kansas at this time (as observed by the dense radiosonde network in operation during STORM-FEST). The maximum wind speed in the jet was 23 m s^{-1}. The Doppler velocity data show that there was a strong, low-level wind directed uniformly toward the radar. However, these velocity data are not characteristic of the velocity signature associated with a squall line that is forced by boundary layer flow, since there is little evidence of low-level convergence (i.e., no gust front signature). This suggests that the rainband was generated by processes occurring above the 850-mb level.

To determine the steering level of the radar echoes associated with the pre-drytrough rainband, we used 15-min radar reflectivity data from the composite NWS digitized radar data, collected within the STORM-FEST observational domain, to trace the motion of precipitation cores from 2301 UTC 8 March to 0115 UTC 9 March. This analysis showed that the cores were moving from between 186° and 191° at a speed between 16.7 and 19.4 m s^{-1}. The 0000 UTC 9 March sounding from Topeka contained only two layers with this wind velocity: one between 930 and 900 mb and the other from 710 to 700 mb. Since the lower level was precluded from consideration based on the Doppler velocity data, the steering level for this rainband must have been near 700 mb. In view of the velocity signature shown in Fig. 3c, the rainband was likely generated between about 800 and 700 mb as an elevated band of strong convection. We will see that these conditions persisted throughout the history of the pre-drytrough rainband.

After 0000 UTC 9 March, the eastern portion of the pre-drytrough rainband continued its gradual movement to the northeast, so that by 0235 UTC 9 March this portion of the band stretched from Kansas City southeastward to the Arkansas–Tennessee–Mississippi border (Fig. 4). However, by this time the rainband was considerably less convective along much of its length. Also, by this time, a severe squall line had developed along the surface drytrough (Fig. 4) and subsequently raced eastward away from the drytrough. This squall line was linked to an upper-level baroclinic zone, which moved ahead of the drytrough as depicted in the cold frontogenesis aloft (CFA) conceptual model of Hobbs et al. (1990). The evolution of this convection, and its role in the overall development of the cyclone, will be discussed in a future paper in this series. The widespread precipitation over the northern plains states, which eventually subsumed the northwestern portion of the pre-drytrough rainband, was associated with the arctic front.

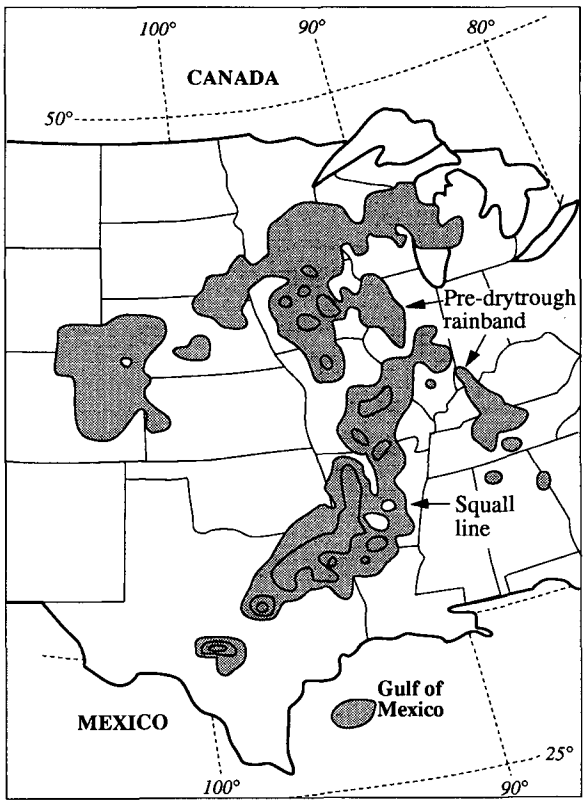

FIG. 5. As for Fig. 1 but for 1035 UTC 9 March 1992.

After 0235 UTC 9 March, the pre-drytrough rainband began to lose its coherent structure. This trend eventually led to its dissolution into a collection of scattered cells, as shown by the NWS radar summary for 1035 UTC 9 March (Fig. 5). After this time, it could no longer be classified as a rainband. Thus, the pre-drytrough rainband, some 1500 km in length at its maximum extent, lasted for 16 h during the evolution of the cyclonic storm in which it was embedded. During this time period, the average precipitation rate associated with the rainband was approximately 1 mm h^{-1} but locally heavier rates were not uncommon. Since the pre-drytrough rainband had an average width of about 75 km, and progressed along its entire length to the northeast, it affected hundreds of thousands of square kilometers in the central United States.

5. Synoptic structure and mechanisms for the development of the pre-drytrough rainband

In the previous section we showed that the pre-drytrough rainband was convective in nature and was generated at middle-tropospheric levels (near 700 mb). In this section we describe the synoptic-scale structure that was responsible for the creation of this rainband. We begin by showing a series of 500-mb maps and discussing the dynamics of a potent upper shortwave associated with the cyclone.

a. Horizontal analyses

A cutoff low at 500 mb, characterized by considerable baroclinicity on its southeastern quadrant, was located over southern California and Arizona at 1200 UTC 8 March (Fig. 6a). This was the first in a series of several strong upper-level disturbances that characterized the Super Tuesday storm. This feature had raced southward in a strong northerly flow just off the Pacific coast on 6 and 7 March 1992. The strong temperature gradient associated with the vorticity maximum, along with a marked decrease in wind speed from northern New Mexico to Colorado, indicated that this feature was associated with significant divergent flow aloft. Consequently, a surface cyclone developed in southwest Colorado in response to the large-scale, but locally intense, synoptic-scale lifting associated with this wave.

By 1800 UTC 8 March, the wavelength between the upper-level trough axis and the downstream ridge axis had shortened, a result of the stationary nature of the ridge axis at 500 mb. An important consequence of this configuration was that the synoptic-scale dynamics of the wave (i.e., positive vorticity advection) were intensified as curvature in the flow created ageostrophic divergence downstream of the trough axis at middle- and upper-tropospheric levels, which created the synoptic-scale region of upward vertical motion in which the pre-drytrough rainband formed (Fig. 6b).

Returning to 700 mb, which was the steering level of the rainband, we show in Fig. 7a series of analyses of 700-mb geopotential heights and temperatures at 6-h intervals taken from MM4 case B simulation beginning at 1200 UTC 8 March and ending at 1200 UTC 9 March. Also shown in Fig. 7 are the corresponding NWS radar summaries depicting the pre-drytrough rainband. The model simulations are in excellent agreement with the (poorer resolution) observational analyses. At 1200 UTC 8 March (Fig. 7a), weak warm-air advection was occurring over Oklahoma, extreme northeastern Texas, and Arkansas in a broad south-

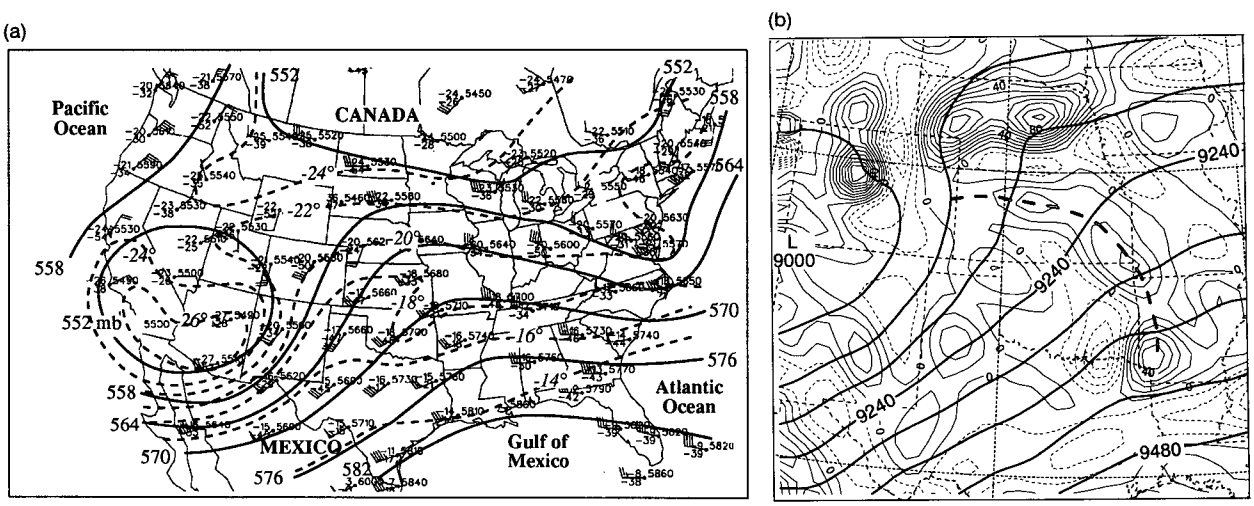

FIG. 6. (a) The 500-mb analysis for 1200 UTC 8 March 1992. Solid lines are geopotential height (dam, contoured every 6 dam). Dashed lines are isotherms (°C, contoured every 2°C). Wind speeds are indicated by: long barb, 5 m s^{-1}; short barb, 2.5 m s^{-1}; and flag, 25 m s^{-1}. (b) MM4 12-h forecast valid at 0000 UTC 9 March 1992 of 300-mb geopotential height (m, thick solid lines, and contoured every 60 m) and 300-mb horizontal divergence (convergence)—thin solid (dashed) lines, labeled in inverse seconds and contoured every 10×10^{-5} s^{-1}. Thick dashed line indicates axis of 300-mb divergence associated with the pre-drytrough rainband.

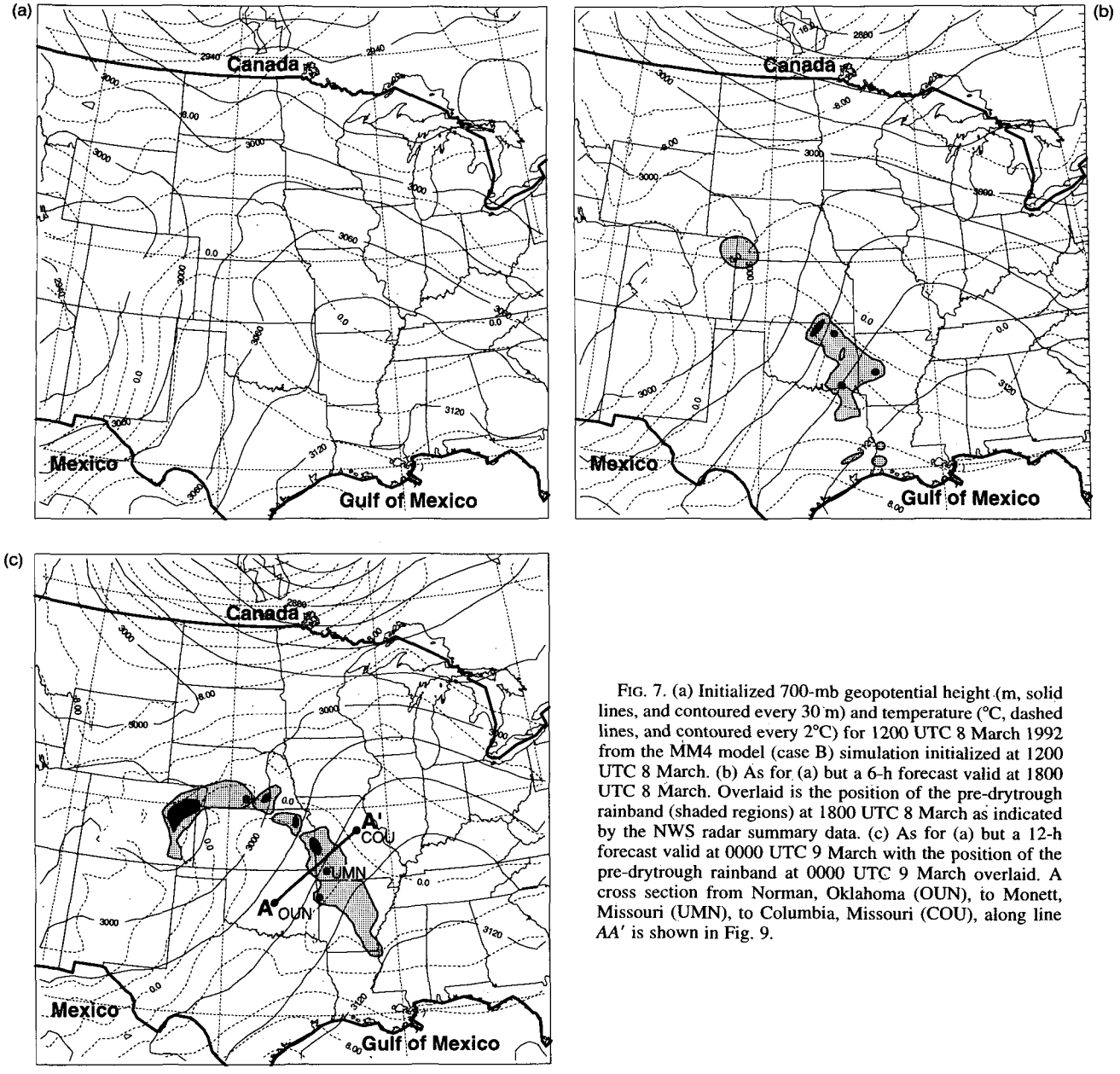

FIG. 7. (a) Initialized 700-mb geopotential height (m, solid lines, and contoured every 30 m) and temperature (°C, dashed lines, and contoured every 2°C) for 1200 UTC 8 March 1992 from the MM4 model (case B) simulation initialized at 1200 UTC 8 March. (b) As for (a) but a 6-h forecast valid at 1800 UTC 8 March. Overlaid is the position of the pre-drytrough rainband (shaded regions) at 1800 UTC 8 March as indicated by the NWS radar summary data. (c) As for (a) but a 12-h forecast valid at 0000 UTC 9 March with the position of the pre-drytrough rainband at 0000 UTC 9 March overlaid. A cross section from Norman, Oklahoma (OUN), to Monett, Missouri (UMN), to Columbia, Missouri (COU), along line *AA'* is shown in Fig. 9.

westerly flow off the Mexican Plateau. Notice the pronounced region of warm air that existed over much of Texas at this time. No radar echoes were reported in this region by the NWS, although there were reports of scattered light rain over southeast Texas.

The scattered showers continued to expand and intensify and by 1535 UTC 8 March they covered most of eastern Texas (Fig. 1). By 1800 UTC, the previously mentioned region of warm air at 700 mb had moved to the northeast and the pre-drytrough rainband was aligned along its eastern edge (Fig. 7b). This corresponded to the warm edge of a region of concentrated warm-air advection at that level. A dynamically important characteristic of this region of warm-air advection is that it occurred in a different horizontal wind field and so was characterized by geostrophic frontogenesis. The 700-mb **Q** vectors (not shown) were directed across the isotherms from cold air to warm air indicating the presence of a thermally direct vertical circulation with upward vertical air motion on the warm edge of the 700-mb temperature gradient. Thus, the warm-air advection region depicted in Fig. 7 enhanced the upward vertical motion that occurred in the rainband environment. Additional model and observa-

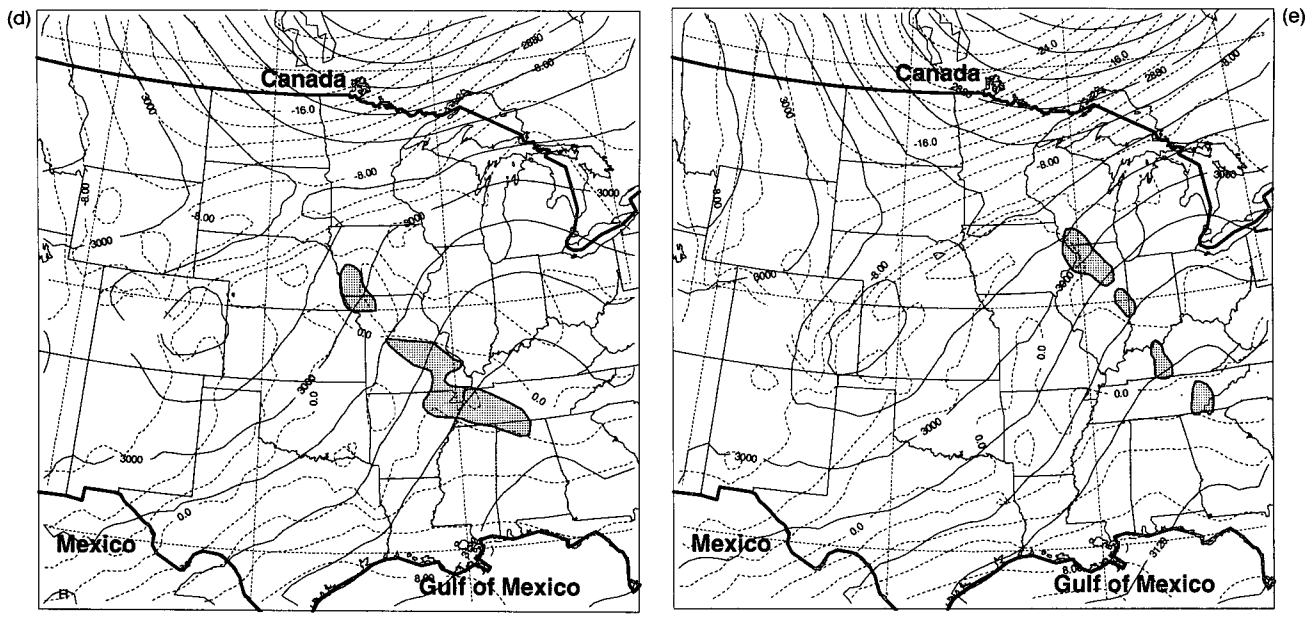

FIG. 7. (*Continued*) (d) As for (a) but for an 18-h forecast valid at 0600 UTC 9 March 1992. Overlaid is the position of the pre-drytrough rainband at 0600 UTC 9 March as indicated by the NWS radar summary data. (e) As for (a) but for a 24-h forecast valid at 1200 UTC 9 March 1992. Overlaid is the position of the pre-drytrough rainband at 1200 UTC 9 March as indicated by the NWS radar summary data.

tional data (not shown) indicated that there was no warm-air advection at 850 mb and only very weak warm-air advection at 500 mb in association with the rainband. By 0000 UTC 9 March (Fig. 7c), when the rainband was at its peak intensity, there was still a good correlation between warm-air advection at 700 mb and the pre-drytrough rainband. By 0600 UTC the region of warm-air advection at 700 mb had become much more diffuse and the rainband had weakened (Fig. 7d). By 1200 UTC 9 March, continued weakening resulted in the dissolution of the pre-drytrough rainband into scattered cells that bore only a very weak relationship to the thermal advection pattern which had, by this time, deteriorated to almost nothing (Fig. 7e). Thus, when the region of warm-air advection (i.e., geostrophic frontogenesis and associated upward vertical motion) weakened, so did the pre-drytrough rainband.

Further evidence for the connection between warm-air advection and the pre-drytrough rainband is shown in Fig. 8, which is a time series of winds from the Neodesha, Kansas, wind profiler. Neodesha was one of a dense network of wind profilers used in STORM-FEST, its location is shown in Fig. 2b. Enclosed within the dotted line in Fig. 8 was a layer where the wind speed was strong and the wind direction uniform. This layer deepens with time beginning at 1500 UTC 8 March and disappears (after deepening to the surface) at 2200 UTC 8 March. As indicated by the Chanute, Kansas, surface observations, the period when this layer was deepening ends with the passage of the pre-drytrough rainband overhead, accompanied by gusty surface winds. The layer of strong winds is the low-level jet; it is capped by a layer of warm-air advection, as indicated by the strong veering of the wind (presumed to be close to geostrophic balance at heights near 2 km) with height above the jet. This region of warm-air advection begins near 2 km at 1200 UTC and rises rather uniformly to about 3 km (its maximum height) at the time of rainband passage. The layer of veering winds then drops abruptly to the boundary layer at 2200 UTC. The relationship between this elevated, sloping zone of warm-air advection and the pre-drytrough rainband is consistent with our previous interpretation that this rainband was generated in a region of frontogenetical warm-air advection at middle levels. The position of the low-level jet in relation to the warm-air advection, and therefore to the pre-drytrough rainband, is discussed later in this paper.

b. Cross section and sounding analysis

The synoptic-scale lifting described above occurred over a broad area within the cyclone. Yet, the pre-drytrough rainband was quite narrow (~75 km). Therefore, the synoptic-scale lifting must have acted on a mesoscale environment, perhaps one susceptible to a flow instability on the scale of 50–100 km. The nearly parallel orientation of the pre-drytrough rainband to the isotherms near 700 mb (Figs. 7c,d) suggests that conditional symmetric instability (CSI) may have been responsible for production of the rainband. To determine if CSI existed in the vicinity of the pre-drytrough rainband we constructed a series of cross sections, one of which is shown in Fig. 9.

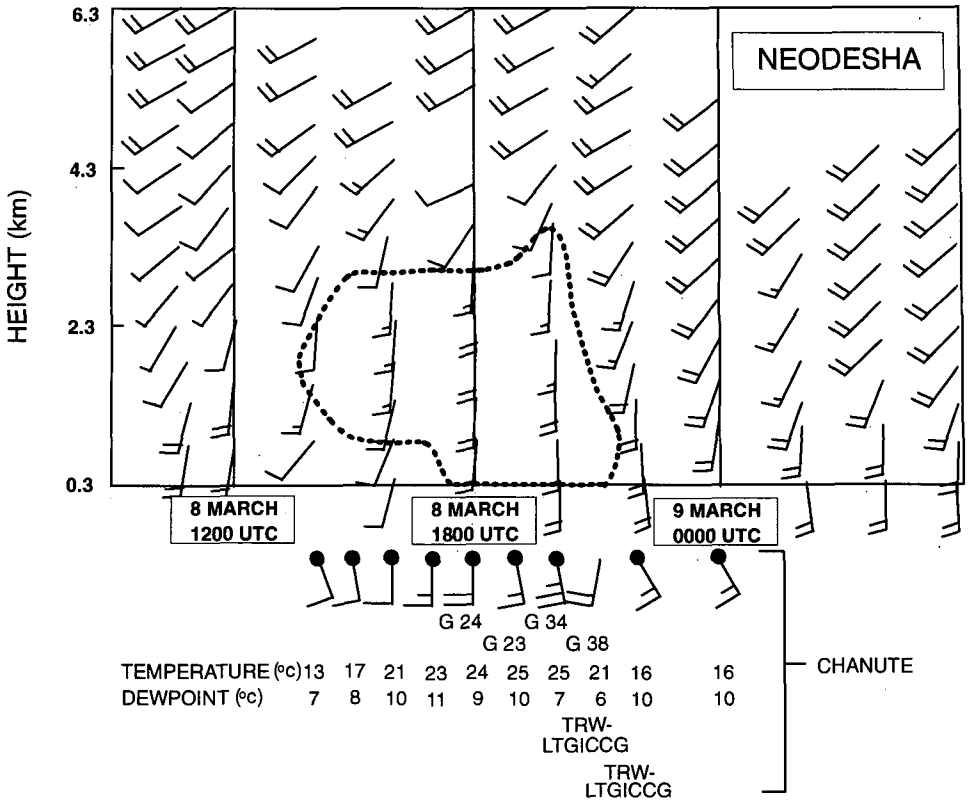

FIG. 8. One-hourly time series of wind measurements from the Neodesha wind profiler from 1000 UTC 8 March to 0300 UTC 9 March 1992. Dotted line encloses the winds associated with the low-level jet. Surface hourly observations for Chanute, Kansas, from 1400 UTC 8 March to 0000 UTC 9 March 1992 are shown at the bottom of the figure ("G" indicates gusts, TRW– indicates a light thundershower, and LTGICCG indicates in-cloud and cloud-to-ground lightning).

Figure 9 is a cross section, along line AA' in Fig. 7c, from Norman, Oklahoma (OUN), to Monett, Missouri (UMN), to Columbia, Missouri (COU), of equivalent potential temperature θ_e at 0000 UTC 9 March 1992. This cross section is perpendicular to the orientation of the pre-drytrough rainband and the 700-mb isotherms at that time. Figure 9 shows the presence of a convective instability (which is a particular form of CSI), which is indicated by the hatched area in Fig. 9. A considerable portion of the cross section is characterized by convective instability, with a particularly deep layer occurring at OUN. The tongue of high θ_e along the sloping base of the convectively unstable layer will be discussed later.

The convectively unstable stratification described above provides the potential for precipitation, but this layer must be lifted by an appropriate amount to release this potential. The soundings comprising the cross section in Fig. 9 can be used to determine the amount of lifting required to release the instability. Since the sounding at Monett (Fig. 10a) was within the rainband at 0000 UTC 9 March, it was not included in the analysis. This sounding does, however, provide further evidence that the pre-drytrough rainband was an elevated convective rainband, since the layer from 700 to 500 mb is nearly saturated and convectively unstable. We will examine the origin of the air in this layer shortly. Using the Norman (OUN) and Columbia (COU) soundings, we determined which 50-mb layer (between 800 and 600 mb) was least resistant to free convection. We chose the 800–600 interval since the rainband was associated with midlevel lifting.

For the sounding at Norman (Fig. 10b), the layer with the least resistance to free convection was between 800 and 750 mb, which required approximately 70 mb of lifting to initiate convection. At Columbia (Fig. 10c), the 700–650-mb layer was most susceptible to free convection; approximately 55 mb of lifting was enough to initiate free convection in this layer.

Since rather small amounts of lifting were required to initiate convection at midlevels at both Norman and Columbia (where it was *not* precipitating), we decided to trace the origin of the midlevel air that produced convective precipitation over Monett at 0000 UTC 9 March. Using the MM4 model (case B) gridded data at 15-min intervals, backward trajectories were calcu-

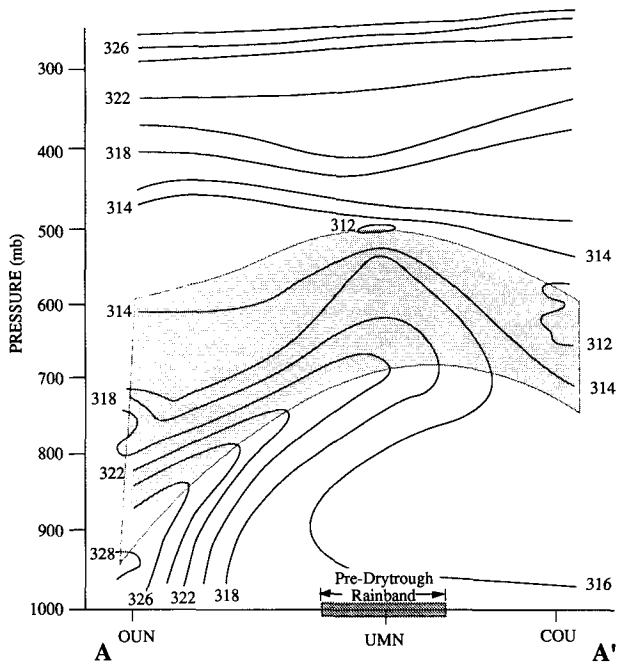

FIG. 9. Cross section (along line AA' in Fig. 7c) from Norman, Oklahoma (OUN), to Monett, Missouri (UMN), to Columbia, Missouri (COU), at 0000 UTC 9 March 1992. Solid lines are equivalent potential temperature θ_e (K, contoured every 2 K) and the shaded area represents region of convective instability.

lated to investigate the origin and evolution of the convectively unstable layer in the Monett sounding at 0000 UTC 9 March. The trajectories were initialized at Monett at 0000 UTC 9 March at 50-mb intervals between 900 and 600 mb and run backwards for 6 h. The results are shown in Fig. 11, where it can be seen that the wind veered with height, indicating the presence of large-scale, warm-air advection. The highest three trajectories shown in Fig. 11 (numbered 5, 6, and 7) do not, however, indicate much wind shear in either direction or speed, in spite of the fact that they span a range of 100 mb. The air parcels associated with these three trajectories rose 50 mb (from 750, 700, and 650 mb, respectively) in the southwesterly flow to arrive at their respective positions over Monett. Thus, the 100-mb deep layer from 700 to 600 mb at Monett at 0000 UTC 9 March originated in a 100-mb-deep layer from 750 to 650 mb over southeastern Oklahoma [just to the southeast of Norman, Oklahoma (OUN)] 6 h earlier.

The OUN sounding at 1800 UTC 8 March is shown in Fig. 12. The air in the 750–700-mb layer needed only about 30 mb of lifting to become freely convective, and this air was lifted 50 mb from 1800 UTC 8 March to 0000 UTC 9 March on its way to Monett. Thus, we conclude that the pre-drytrough rainband was formed within a narrow portion of a widespread region of convective instability that was particularly susceptible to free convection. Lifting provided by synoptic-scale warm-air advection, and geostrophic frontogenesis with associated ageostrophic divergence, released this convective instability in the middle troposphere.

6. Evolution of the cyclone containing the pre-drytrough rainband

We have shown that the pre-drytrough rainband was the manifestation of convective instability released in the middle troposphere by upward motion that was forced, in part, by the dynamics of a short-wave trough that intruded from the southwest. In this section we describe the evolution of the cyclone in which this rainband formed. This evolution involved complex interactions between an elevated mixed layer, a low-level jet, and the drytrough, with the latter feature playing a central role. We will show that although these features appeared to be largely distinct from one another, they were in fact intimately related to a single feature that is common to the development of all winter cyclones in the central United States, namely, flow across elevated terrain.

Figure 13a shows the terrain field used in the MM4 model; it approximates the mean elevation of the Rockies and the Mexican Plateau but it does not resolve individual peaks. Figures 13b and 13c show the MM4 case A initialized potential temperature θ field at 0000 UTC 8 March 1992 for two sigma levels. The Rocky Mountains and Mexican Plateau are regions of maximum θ, both near and at some distance above the surface; this is due primarily to the elevated land masses acting as heat sources. The presence of this continental-scale, north–south-oriented axis of high potential temperature, extending through a significant depth of the free atmosphere, has profound effects on the development and structure of baroclinic waves as they pass eastward over the Rockies. These effects stem largely from the fact that during cyclonic development the air with high potential temperature is advected horizontally at different rates in the vertical over the central United States. This leads to significant modification of the large-scale thermal advection pattern. We begin our description of these effects by describing the development of an important feature close to the surface, namely, the drytrough.

a. The lee trough, dryline, and drytrough

Figure 14a shows the sea level pressure analysis for 1200 UTC 8 March 1992. A weak pressure trough at the surface extended southward through eastern New Mexico from a 1000-mb surface low pressure center in southwestern Colorado. This disorganized trough was located in a broad region of maximum surface potential temperature (θ = 294 K) at this time. By 1800 UTC (not shown) the trough had become more organized and higher potential temperature air had entered the trough region. The axis of this warm air was nearly

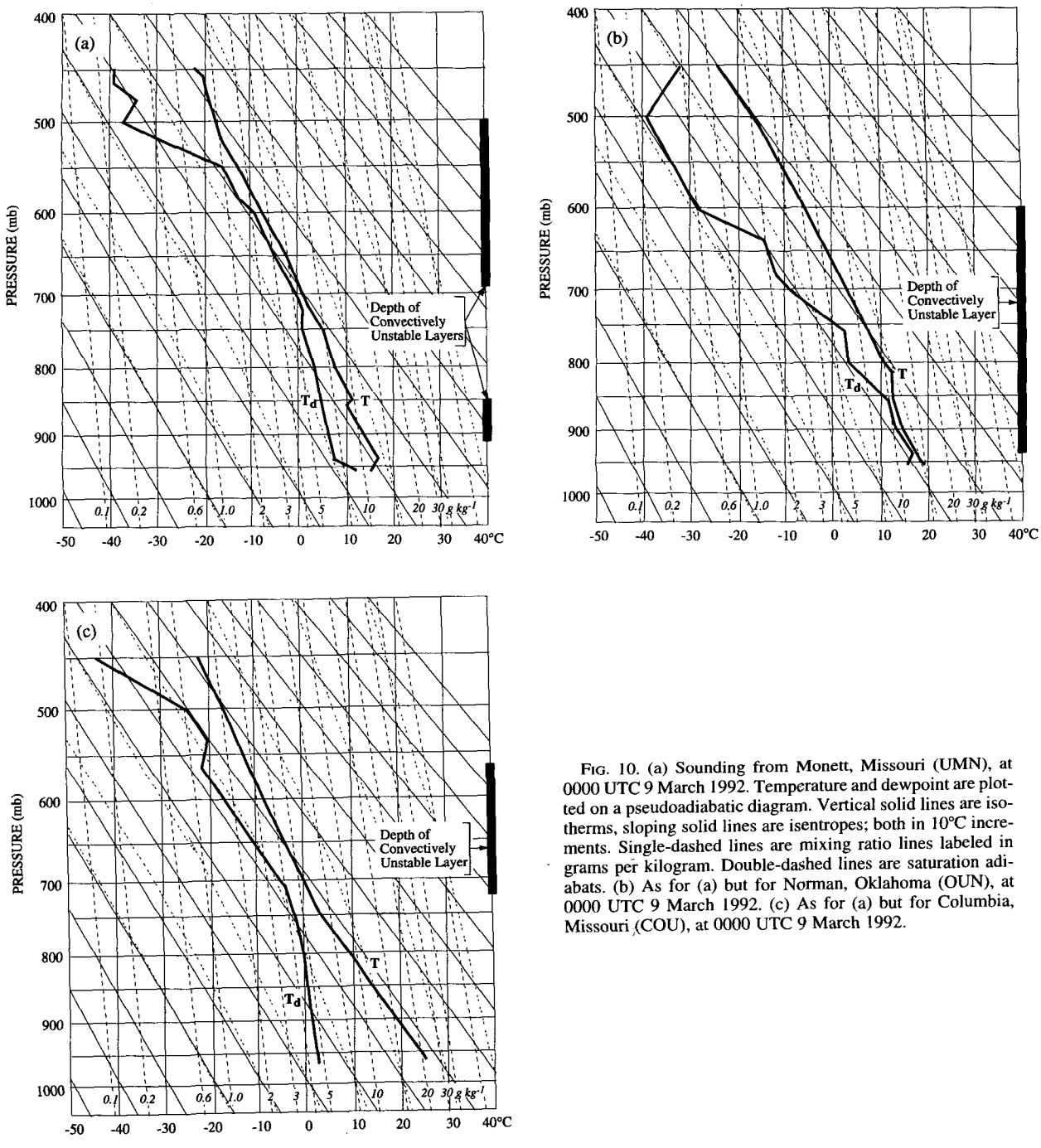

FIG. 10. (a) Sounding from Monett, Missouri (UMN), at 0000 UTC 9 March 1992. Temperature and dewpoint are plotted on a pseudoadiabatic diagram. Vertical solid lines are isotherms, sloping solid lines are isentropes; both in 10°C increments. Single-dashed lines are mixing ratio lines labeled in grams per kilogram. Double-dashed lines are saturation adiabats. (b) As for (a) but for Norman, Oklahoma (OUN), at 0000 UTC 9 March 1992. (c) As for (a) but for Columbia, Missouri (COU), at 0000 UTC 9 March 1992.

coincident with the trough axis. By 0000 UTC 9 March even warmer air had found its way into the center of the now much better organized surface trough (Fig. 14b). Further, the axis of warmest air at the surface was now unquestionably the axis of the trough itself. This thermal structure is a characteristic of leeside troughs.

We used the model output for case B (initialized at 1200 UTC 8 March) to investigate the 3-h pressure falls associated with this developing lee trough. The results (not shown) showed that the strongest intensification of the pressure signal of the lee trough was coincident with an increase in potential temperature along the axis of the lee trough at the surface (which is apparent from Fig. 14). Furthermore, this intensification occurred when the flow in the lower troposphere over the high terrain of Colorado, New Mexico, and west Texas veered from southwesterly to westerly with

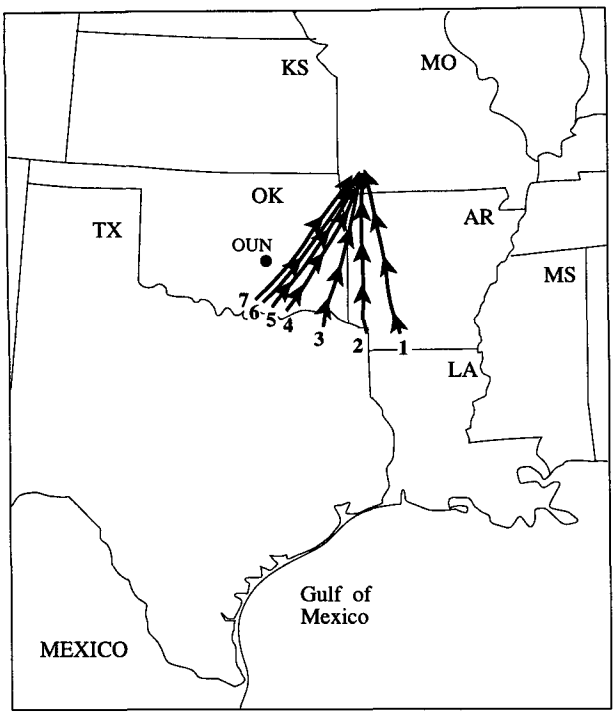

FIG. 11. Series of seven 6-h backward trajectories from the MM4 model (case B) simulation initiated at Monett, Missouri, at 0000 UTC 9 March 1992 at 50 mb intervals from 900 to 600 mb (trajectories 1 to 7, respectively). Notice that trajectories 5, 6, and 7 all originated from the same area and moved along the same horizontal path. Location of Norman, Oklahoma (OUN), is indicated.

the approach and passage of the upper-level synoptic disturbance. This horizontal veering of the winds produced an increased flow of air across the mountain at middle levels, which produced the downward advection of high potential temperature toward lower elevations to the east. Thus, a localized region of air with high potential temperature was created at lower elevations and this low-level warm air maintained a minimum in pressure at the surface.

To demonstrate how the downward advection of air with high potential temperature evolved into a warm tongue of air, we studied eight MM4 model (case B) generated trajectories. Each of these trajectories was run backwards for 9 h from starting points at 850 mb along and to the east of the position of the surface warm anomaly at 2100 UTC 8 March (Fig. 15a). The results are shown in Fig. 15b. Trajectories 1–4 were located along the axis of the surface warm-air anomaly at 2100 UTC; trajectories 5–8 were located approximately 135 km east of this line. Trajectories 1–3 sank about 30 mb before arriving at 850 mb at 2100 UTC 8 March. Trajectory 4 sank only 20 mb to the same isobaric level. Importantly, however, all four of these air parcels were located farther above the ground at 2100 UTC than they were at 1200 UTC 8 March, even though they had sunk to higher isobaric values during this time interval. Therefore, these air parcels had subsided off the high, warm terrain to the west, and advected air with high potential temperature downward toward the surface. This created a subsidence-induced warm tongue of air that maintained a pressure trough at the surface.

Trajectories 5 and 6 rose ahead of the developing lee trough, while trajectories 7 and 8 underwent largely horizontal advection. The differential vertical motion between trajectories along (sinking) and east of (rising) the surface trough strengthened the warm-air anomaly along the axis of the lee trough.

Finally, the extreme values of potential temperature in the surface pressure trough at 2100 UTC (Fig. 15a) were produced, in part, by diabatic heating during the day, as evidenced by their southward retreat after local sunset (not shown). As discussed by Benjamin and Carlson (1986), this diabatic effect serves to strengthen the pressure anomaly manifest in the surface lee trough. However, diabatic heating alone cannot explain the localization of such potentially warm air within the trough axis. This localization at the surface can be explained only by the subsidence described above.

Coincident with the intensification of the leeside surface trough was an increase in the moisture contrast across it. This increase was documented by considering θ_e fields at the surface. The θ_e field at 1200 UTC 8 March is shown in Fig. 16a. At this time there was a moderate θ_e gradient east of the axis of the surface lee trough. Since θ showed no pronounced gradient in as-

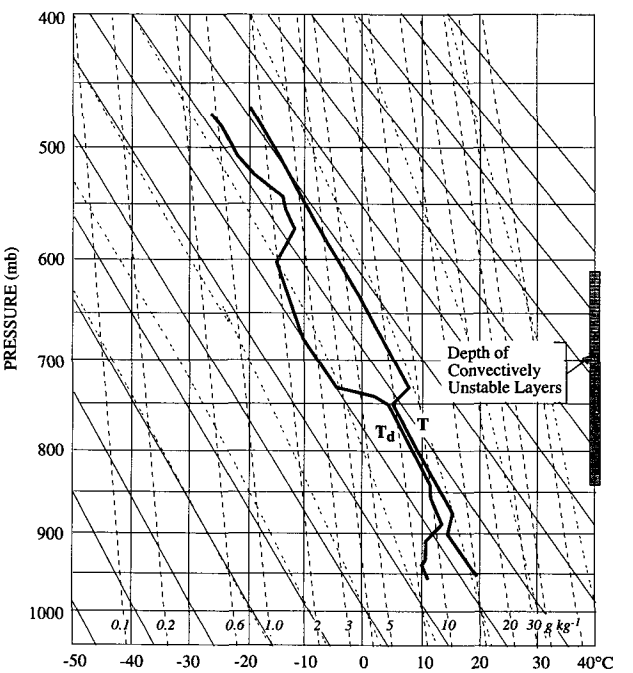

FIG. 12. As for Fig. 10a but for Norman, Oklahoma (OUN), at 1800 UTC 8 March 1992.

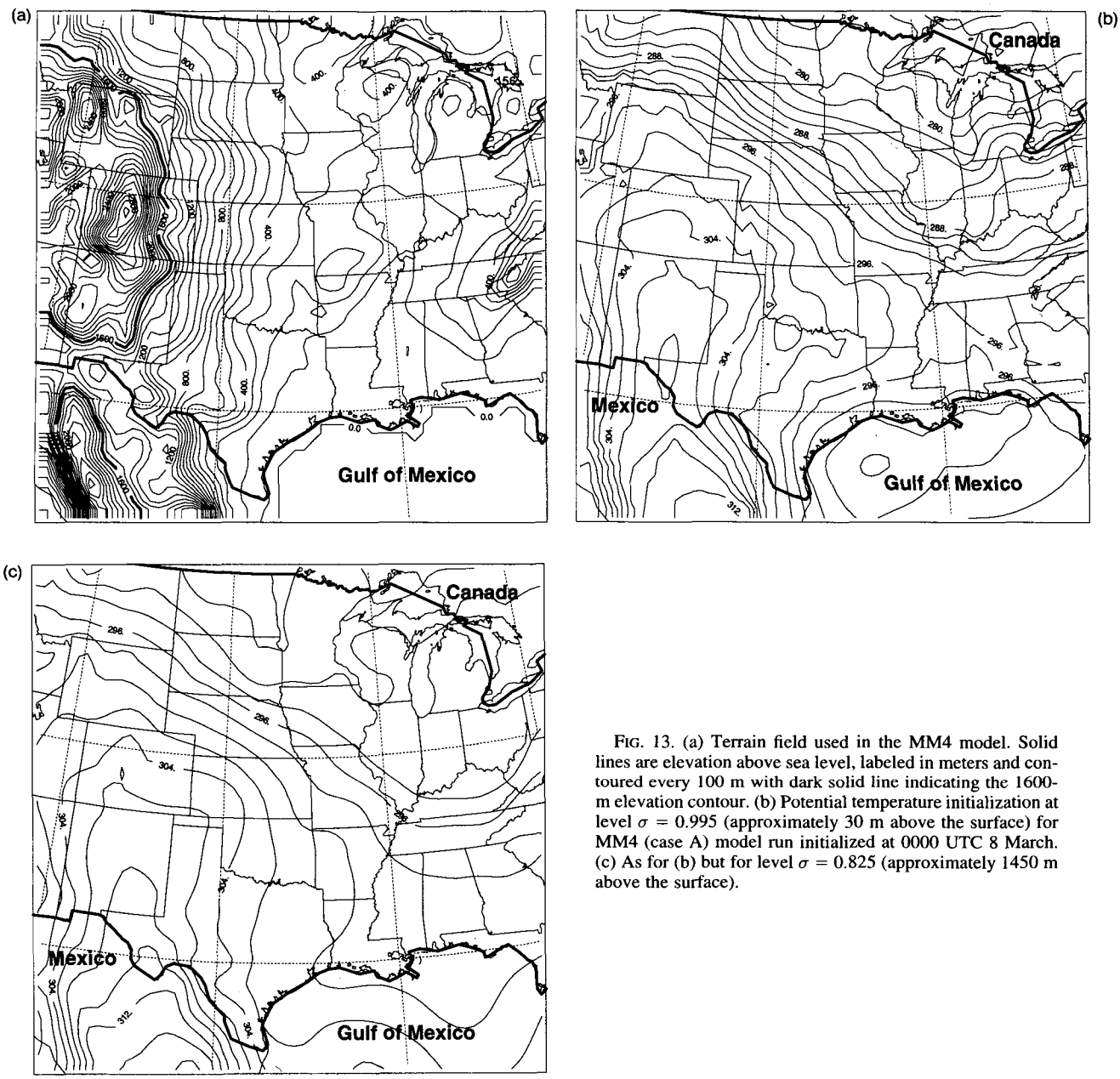

FIG. 13. (a) Terrain field used in the MM4 model. Solid lines are elevation above sea level, labeled in meters and contoured every 100 m with dark solid line indicating the 1600-m elevation contour. (b) Potential temperature initialization at level $\sigma = 0.995$ (approximately 30 m above the surface) for MM4 (case A) model run initialized at 0000 UTC 8 March. (c) As for (b) but for level $\sigma = 0.825$ (approximately 1450 m above the surface).

sociation with this surface trough, the strength of the θ_e gradient must have been due to moisture differences between the air east and west of the lee trough. A further intensification of this gradient had occurred by 1800 UTC (not shown); this trend continued through 2100 UTC (not shown) and up to 0000 UTC 9 March (Fig. 16b), at which time there was a remarkable gradient in θ_e across the surface lee trough. Thus, the developing surface lee trough became a boundary between very moist air to the east and extremely dry air to the west. This is the classic signature of the *dryline* (Schaefer 1986). By 1800 UTC 8 March, the surface trough had acquired the characteristics of both a lee trough and a dryline, and was therefore, in our terminology, a *drytrough.*

The vertical structure of the drytrough (which was driven by synoptic-scale forcing) was of central importance to the development of the pre-drytrough rainband. Figure 17 shows a series of cross sections of θ_e at 6-h intervals along line BB' in Fig. 16a from MM4 (case B) simulations. The northern portion of this cross section is approximately the same as that shown in Fig. 9. A weak but persistent gradient in potential temperature existed just to the east of the drytrough (Fig.

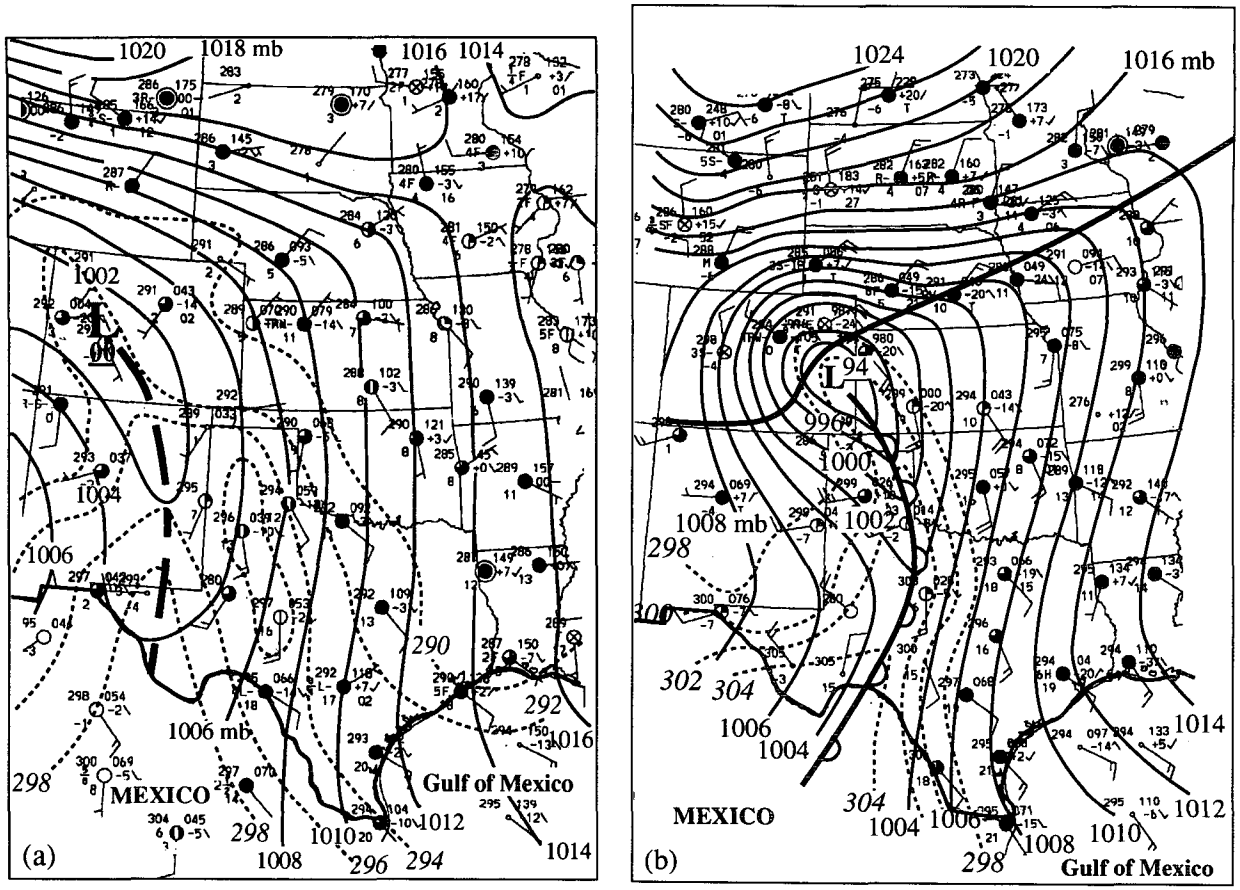

FIG. 14. (a) Sea level pressure and potential temperature analysis for 1200 UTC 8 March 1992. Solid lines are isobars (in mb, contoured every 2 mb) and dashed lines are isentropes (K, contoured every 2 K from 298 to 290 K). The "L" marks the position of the low pressure center at the surface. The heavy dashed line shows the position of the lee trough. For each surface station the following data are shown: potential temperature (K, upper left of the station symbol), dewpoint temperature (°C, lower left of station symbol), sky cover (in center of station symbol), wind direction and speed, and present weather. Sky cover is shown using the following symbols: open circle, clear; half-circle shaded, scattered cloud; unshaded vertical strip within otherwise shaded circle, broken cloud; fully shaded circle, overcast; and X, sky obscured. Wind speeds are indicated by: circle around a circle, calm; long barb, 5 m s^{-1}; short barb, 2.5 m s^{-1}; and flag, 25 m s^{-1}. Present weather symbols: R (rain), W (shower), L (drizzle), H (haze), S (snow), F (fog), ZR (freezing rain), BS (blowing snow), and K (smoke). A plus (+) or minus (−) sign after the precipitation type indicates heavy or light precipitation, respectively. (b) As for (a) but for 0000 UTC 9 March with potential temperature analyzed from 304 to 298 K.

14b). This gradient was subjected to the confluent wind field associated with the trough itself, and a maximum in frontogenesis was produced at low levels (not shown) where it was attended by a shallow, warm frontal–like vertical circulation. This circulation was responsible for a gradual vertical protrusion of high-θ_e air (Figs. 17a–c), originally confined to the lowest levels (Fig. 17a), into a tongue that projected into the middle troposphere by 0000 UTC 9 March (Fig. 17c).

The lee trough can develop warm-frontal characteristics (Carlson 1961; Locatelli et al. 1989; Martin et al. 1990; Steenburgh and Mass 1994). In the case described here, the weakness of the warm-frontal characteristics exhibited by the drytrough was a result of meager preexisting baroclinicity east of the trough. Notwithstanding the relative weakness of these characteristics, Fig. 17 shows that the vertical circulation associated with the drytrough was responsible for the creation of the convectively unstable region at middle levels, which was required for the development of the rainband.

Martin et al. (1990) suggested that the lee trough and the dryline are seasonally dependent manifestations of a basically similar physical process, namely, subsidence in the lee of the Rockies. We have shown that the drytrough in the case discussed here began as a leeside surface trough. As the drytrough was intensified by increased across-mountain flow, the convergence and confluence associated with it also increased. The invigorated horizontal deformation field at the surface, acting on the moisture gradient between the Gulf coast of Texas and west Texas, increased the gradient of

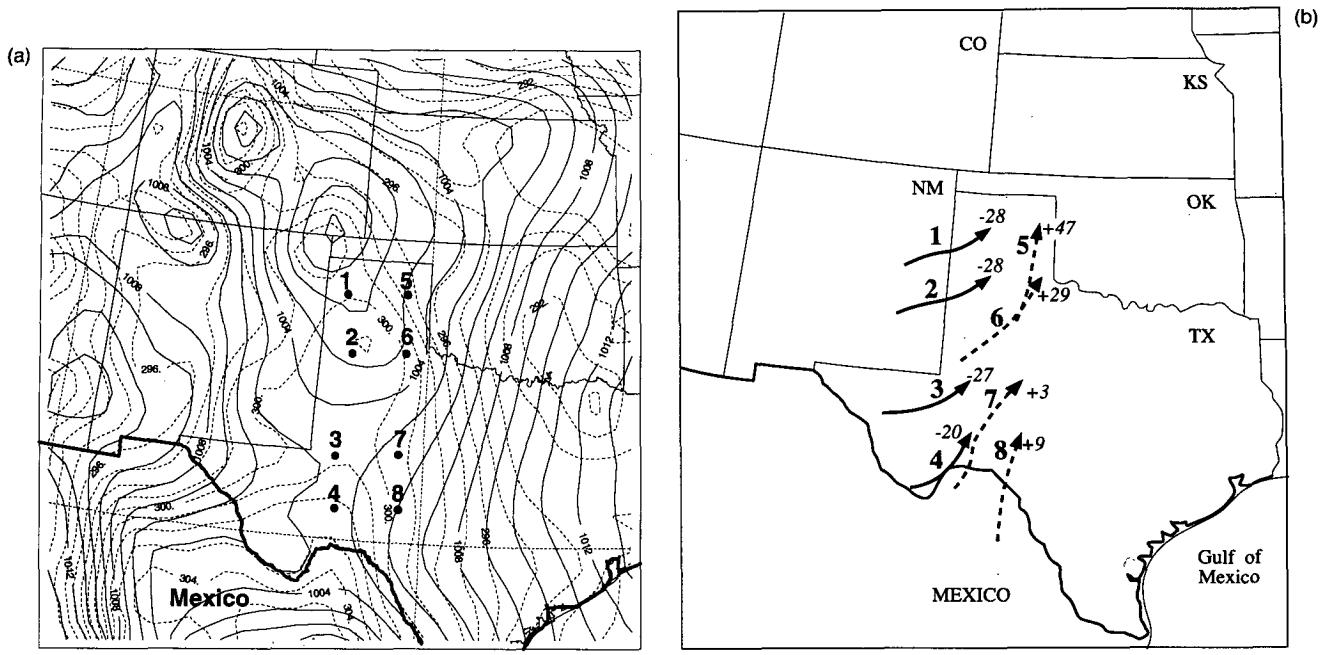

FIG. 15. (a) Nine-hour forecast of sea level pressure (mb, solid lines, and contoured every 1 mb) and potential temperature (K, dashed lines, and contoured every 1 K) at $\sigma = 0.995$ from the MM4 model (case B) simulation valid at 2100 UTC 8 March 1992. Points labeled 1–8 represent horizontal positions of end points for backward trajectories shown in Fig. 15b. (b) 9-h back trajectories calculated using MM4 model (case B) simulation from 1200 UTC to 2100 UTC 8 March to their respective ending points, at 850 mb. Solid arrows represent sinking trajectories with the magnitude of sinking (in millibars) indicated in italics. Dashed lines represent rising trajectories with the magnitude of the rising (in millibars) indicated in italics.

moisture across the trough axis and simultaneously created a shallow, frontogenetically driven vertical circulation. Two important consequences of this process were the creation of a moisture gradient (characteristic of a dryline) in association with the lee trough, and the thrusting of a vertical plume of moisture into the middle troposphere. The surface effect is consistent with Schaefer's (1986) statement that the "dryline itself forms through a frontogenetic process." However, Schaefer also states that although the dryline is "often associated with a pressure trough and/or wind shift line, neither feature is necessary for dryline existence." On the contrary, we believe that a deformation field is necessary to intensify the moisture gradient across the dryline and that this deformation field is provided by the surface leeside trough. It is possible to have a lee trough with no dryline only if there is insufficient moisture contrast across the lee trough. However, a dryline cannot exist without an associated lee trough. For example, a careful analysis of the retrogressing dryline studied by Parsons et al. (1991) shows that it was associated with a lee trough.

b. The low-level jet

The drytrough discussed above was associated with an important horizontal circulation that can be linked to the low-level jet. In section 4 we saw that a portion of the pre-drytrough rainband was located above this low-level jet (LLJ). Here we investigate how the LLJ fits into the overall cyclonic structure.

Surface pressure falls in the high terrain of west Texas and eastern Colorado cause local accelerations of the wind. This increases the magnitude of the ageostrophic wind component east of the trough axis. If the wind accelerations are prolonged, a narrow zone of strong low-level winds develops. This feature, when isolated in the vertical, is known as the LLJ; it is as ubiquitous and important in the development of cyclones in the central United States as is the leeside trough. In fact, Djuric and Damiani (1980) state that: "The low-level jet is the most important mechanism for supplying water vapor and latent heat for the middle-latitude storms of North America." Djuric and Damiani present a conceptual model for the development of the LLJ and note that it occurs in 90% of soundings that are located east of a surface trough and that exhibit a prevailing southerly wind.

Figure 18 shows the position of the wind speed maximum at 850 mb at 1200 UTC 8 March and 0000 UTC 9 March as represented by the MM4 (case B). The core of the LLJ was always below 850 mb although it fluctuated with time. The LLJ migrated northward from central Texas at 1200 UTC (Fig. 18a) to the Kansas–Missouri–Oklahoma border by 0000 UTC 9 March (Fig. 18b). This zone of maximum low-level wind

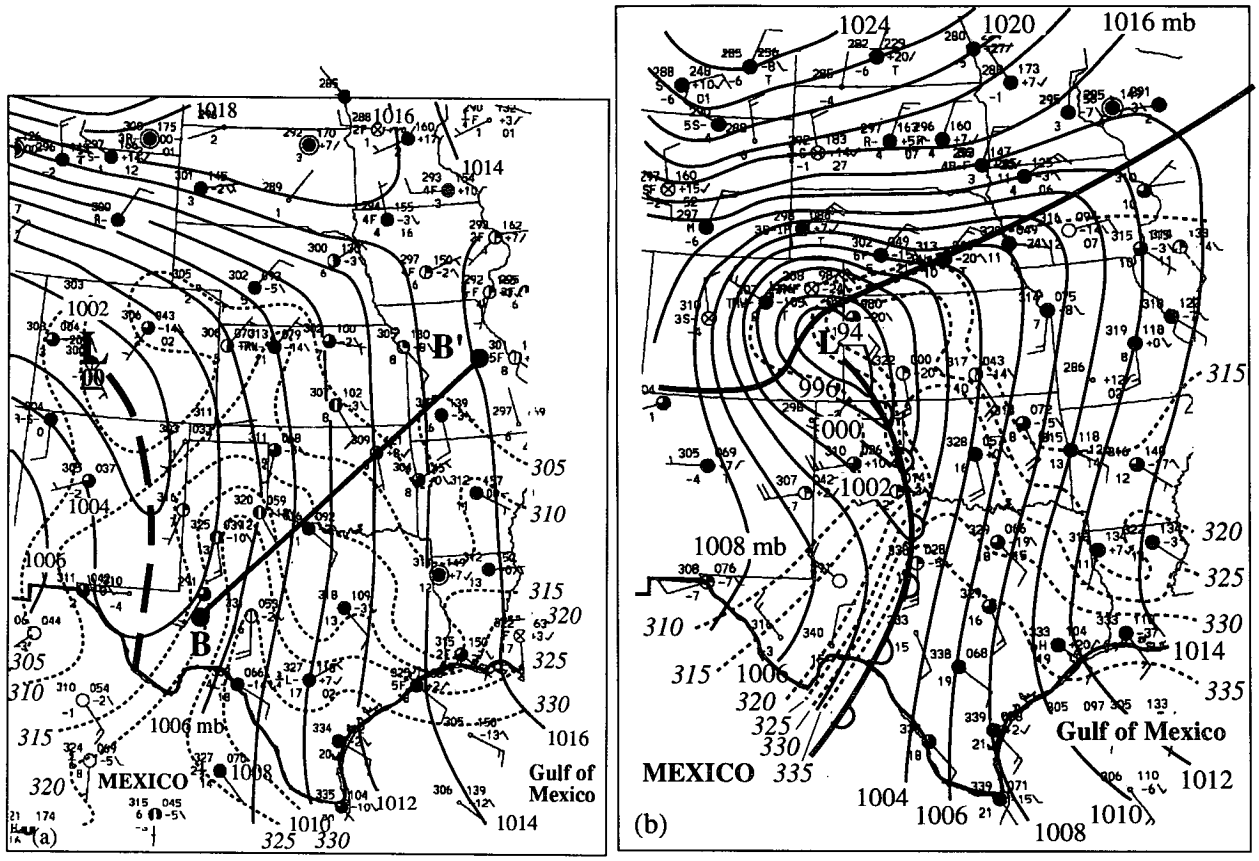

FIG. 16. (a) As for Fig. 14a except equivalent potential temperature θ_e is indicated to the upper left of the station circle and the dashed lines are equivalent potential temperature θ_e, labeled in kelvins and contoured every 5 K from 330 to 305 K. Dashed line indicates position of sea level pressure trough. (b) As for (a) except for 0000 UTC 9 March 1992 with θ_e contoured from 335 to 310 K. Heavy solid and scalloped lines indicate the positions of the arctic front and the drytrough, respectively.

speeds occurred east of the drytrough and was the most vigorous portion of the organized, synoptic-scale horizontal flow associated with the drytrough. It was responsible for the ingestion of large amounts of water vapor and latent heat into the evolving storm system.

The core of the LLJ almost always appears at the base of an inversion layer (Djuric and Damiani 1980), as does the moist air east of the dryline (Schaefer 1974). In the present case, the LLJ was confined beneath an inversion capped by a region of warm-air advection. The inversion layer and the warm-air advection were related to the presence of a warm pool of air at middle levels, the eastern edge of which represented the middle tropospheric, warm-air advection zone that provided the lifting required for the generation of the pre-drytrough rainband.

c. *Development of the warm pool of air at middle levels*

The vertical thermal structure over the southwestern United States and northern Mexico at 0000 UTC 8 March is shown in Fig. 13. A deep pool of warm air existed over the Rocky Mountains and the Mexican Plateau. As the synoptic-scale, baroclinic wave associated with the cyclone moved over the warm air, there was differential horizontal advection of the air with a high potential temperature. Figure 19 shows the 18-h forecast from the MM4 (case A) of 750-mb geopotential heights and isotherms valid at 1800 UTC 8 March. The positions of six air parcels are indicated in Fig. 19, all of which are located along the axis of highest potential temperature at this level. At 750 mb the axis of the warm air was considerably farther east than the corresponding axis at the surface (which constituted the axis of the drytrough). Figure 20 shows 18-h back trajectories of the six parcels indicated in Fig. 19. Trajectories 1, 4, 5, and 6 all sank 60–100 mb during their 18-h journey to the axis of highest potential temperature at 750 mb at 1800 UTC 8 March. The overall picture suggests the following evolution. Since baroclinic waves are characterized by vertical shear, the wind speed at and near 750 mb is greater than that near the ground. Thus, the axis of the warmest air at 750 mb

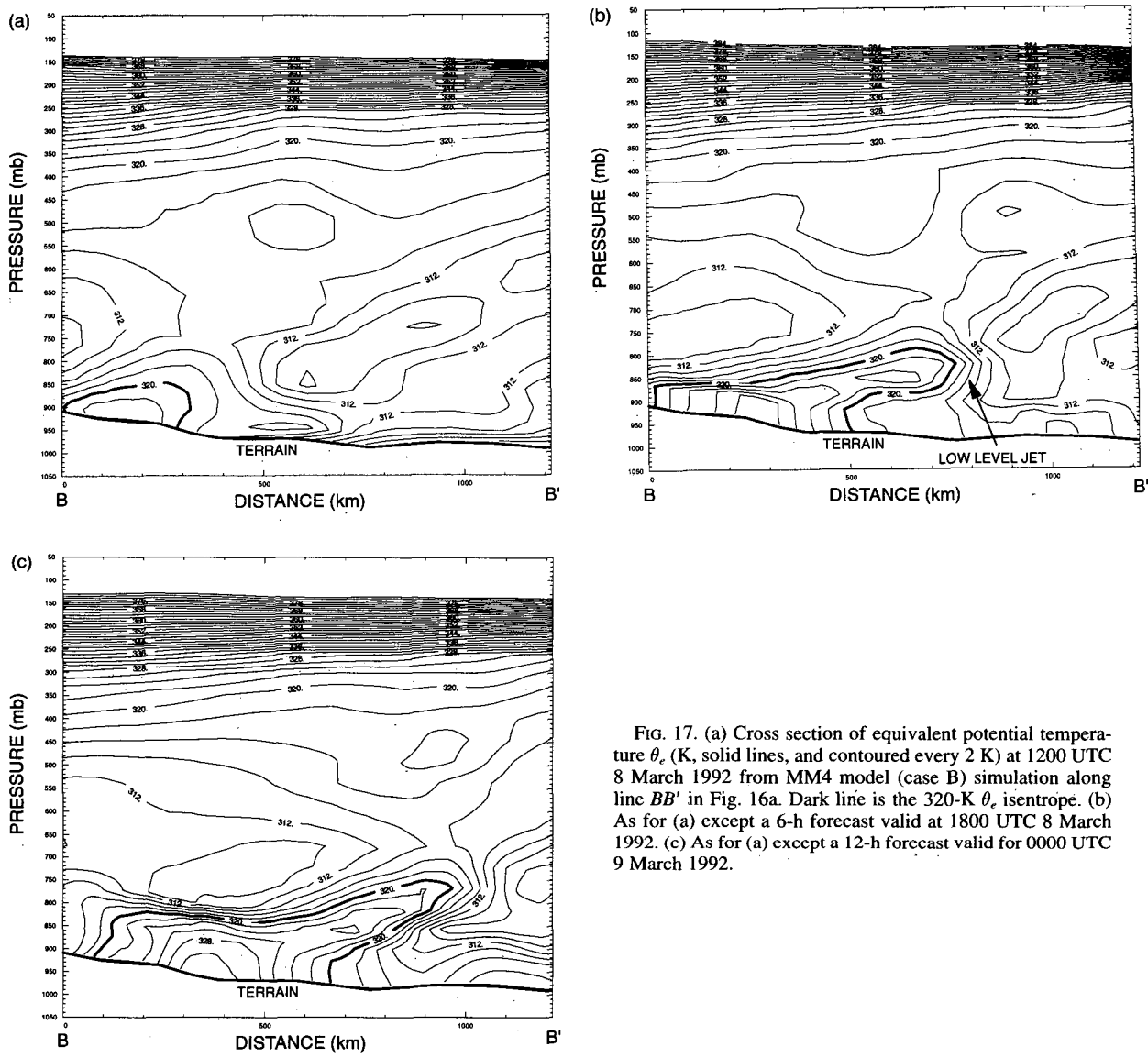

FIG. 17. (a) Cross section of equivalent potential temperature θ_e (K, solid lines, and contoured every 2 K) at 1200 UTC 8 March 1992 from MM4 model (case B) simulation along line *BB'* in Fig. 16a. Dark line is the 320-K θ_e isentrope. (b) As for (a) except a 6-h forecast valid at 1800 UTC 8 March 1992. (c) As for (a) except a 12-h forecast valid for 0000 UTC 9 March 1992.

at 1800 UTC 8 March, which was advected by the synoptic-scale flow into central Texas from its origin over the elevated heating source of the Mexican Plateau, ended up to the east of its counterpart at the surface. In fact, a vertical cross section through the axis of warm air at 750 mb (Fig. 21) shows that the warmest air tipped eastward with height as a result of the differential horizontal advection associated with the upper disturbance. This resulted in what looked like a warm front east of the drytrough. This feature, together with the baroclinic zone intruding from the west in association with the upper shortwave, created the warm occluded–like structure that is evident in Fig. 21, with the drytrough acting as the surface warm front. A similar structure was shown by Carlson and Ludlam (1968, their Fig. 26), Carlson et al. (1983, their Fig. 10), McCarthy and Koch (1982, their Fig. 5), and Schaefer (1986, his Fig. 23.7). The differential vertical motion that occurred on different sides of the axis of warmest air (see caption, Fig. 21) provides further thermodynamic support for the presence of an anomalous tongue of warm air. The presence of such a well-mixed, warm layer of air lying above potentially cooler air over the southeastern United States is accounted for by the differential advection. This scenario is very similar to the conceptual model of the elevated mixed layer presented by Carlson et al. (1983), except that we suggest that the EML is just one component of the larger scale, eastward-tipping, warm-air axis that results from the differential horizontal advection of air during the passage of a baroclinic wave over the elevated terrain of the southern Rockies and Mexican Plateau. In a future pa-

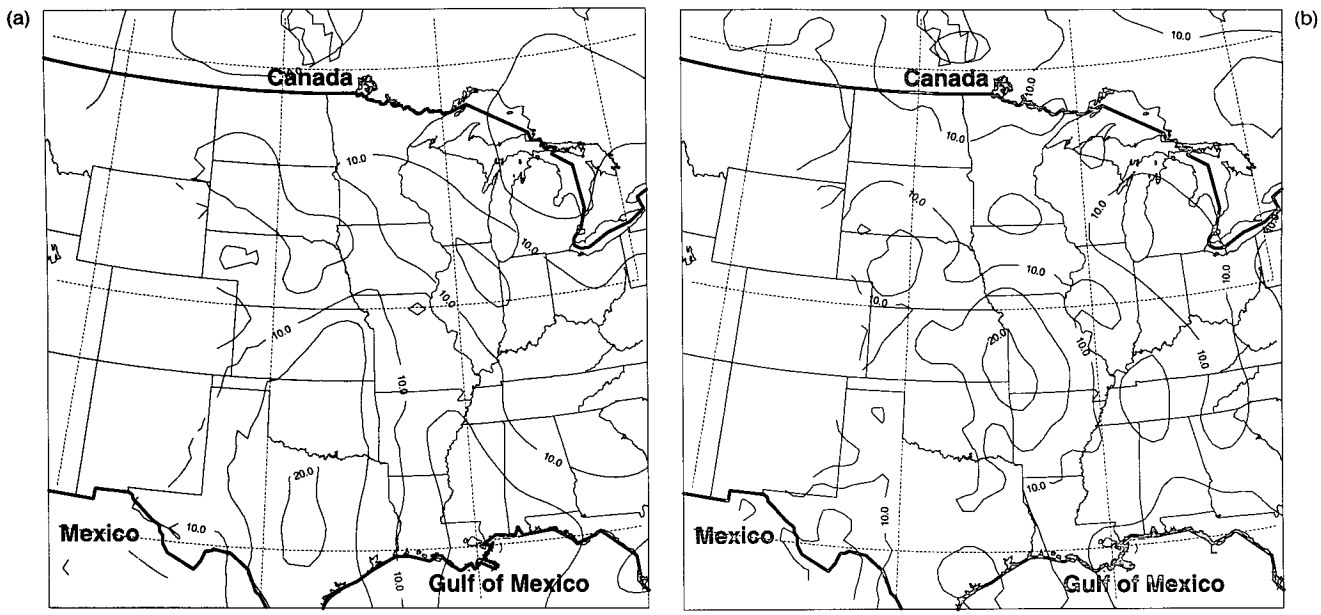

FIG. 18. (a) The 850-mb wind speed (m s^{-1}, solid lines, and contoured every 5 m s^{-1} from MM4 model (case B) initialization valid at 1200 UTC 8 March 1992. (b) As for (a) but a 12-h forecast valid at 0000 UTC 9 March 1992.

per in this series, we will show that the presence of such an EML was a factor in the development of a severe squall line that was generated along the dry-trough at 2100 UTC 8 March.

Shown in Fig. 19 there is a zone of warm-air advection just downstream of the warmest air at 750 mb. The southwestward-directed temperature gradient vector associated with this warm-air advection is underesti-

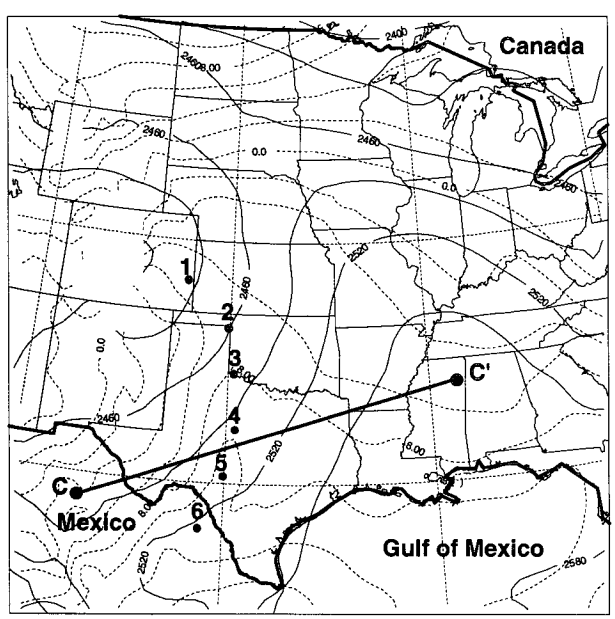

FIG. 19. The 750-mb geopotential height (m, solid lines, and contoured every 30 m) and temperature (°C, dashed lines, and contoured every 2°C) from the 18-h forecast from MM4 model (case A) simulation valid at 1800 UTC 8 March 1992. Points 1–6 are endpoints at 750 mb for trajectories shown in Fig. 20. Cross section along line *CC'* is shown in Fig. 21.

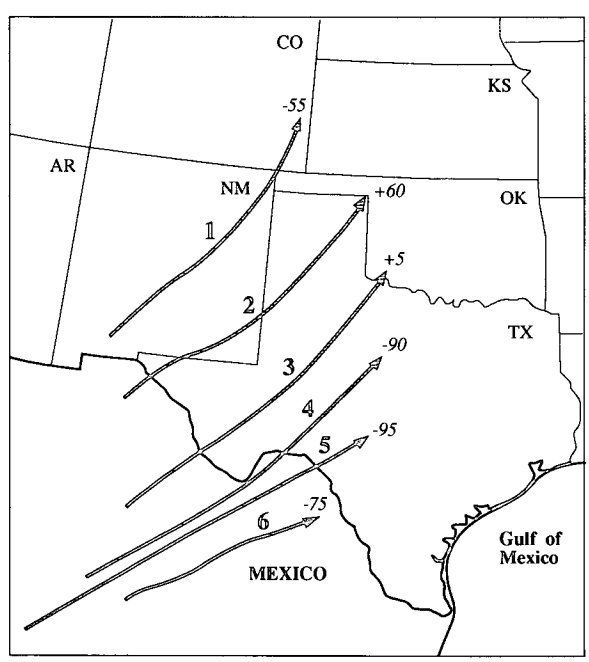

FIG. 20. Eighteen-hour backward trajectories ending at 750 mb at 1800 UTC 8 March at points indicated in Fig. 19. Isobaric change (in millibars) for each trajectory is indicated next to the trajectory endpoint.

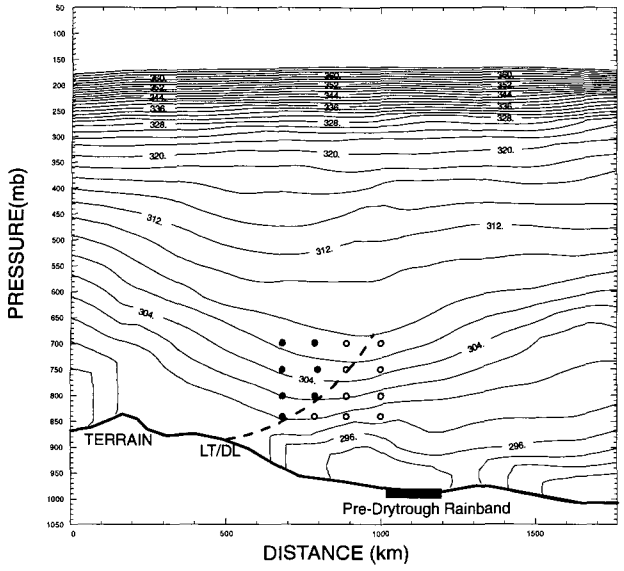

FIG. 21. Six-hour forecast from MM4 model (case B) simulation of potential temperature (K, solid lines, and contoured every 2 K) valid at 1800 UTC 8 March, along line *CC'* in Fig. 19. Dashed line is the sloping axis of warmest potential temperature, which intersects the surface at the drytrough. Open circles are end points of 12-h back trajectories that ascended to those positions. Solid circles are end points of 12-h back trajectories that descended to those positions.

mated in this MM4 model simulation; nevertheless, it suggests a physical explanation for the vertical isolation of the LLJ. The LLJ was located in northeastern Oklahoma at this time. The isotherms in northeastern Oklahoma (Fig. 19) indicate the presence of a predominantly northwesterly thermal wind, which was a direct result of the presence of the warm air just upstream at 750 mb. Thus, as suggested by Palmen and Newton (1969), the LLJ is vertically isolated due to the presence of a deep layer of northerly thermal wind directly above the jet core, which is a consequence of the advection of warm air northeastward off the elevated heat source. Thus, the inversion base where the LLJ is usually located (Djuric and Damiani 1980), can be interpreted as the base of the restraining lid in the EML model of Carlson et al. (1983). Importantly, the presence of a LLJ in predominantly south to southwesterly flow necessitates the presence of a region of warm-air advection at middle levels. This dynamical constraint argues strongly for the recurrence not only of this particular cyclonic structure but also for the pre-drytrough rainband as a common component in winter cyclones in the Midwest. Regular observations of daily weather patterns in the central United States show this to be the case.

7. Discussion

The modifications of cyclonic disturbances that result from their passage over the planetary-scale cordillera of North America can have profound effects on their synoptic and mesoscale structures. These modifications often result in storm structures that deviate significantly from the classical Norwegian cyclone model. For example, the organization of precipitation in cyclones in the lee of the Rockies is often nonclassical (Holzman 1936; Lichtblau 1936; Lloyd 1942; Means 1952). More recently, it has been demonstrated that a class of nonclassical structures characterized by the presence of midlevel frontogenesis can lead to the development of severe weather east of surface pressure troughs (Locatelli et al. 1989; Sienkiewicz et al. 1989; Martin et al. 1990). These observational results are summarized, and a conceptual model is presented for such synoptic-scale structures [known as the cold frontogenesis aloft (CFA) model] by Hobbs et al. (1990). The pre-drytrough rainband that we have described in this paper represents another nonclassical feature. This elevated convective rainband, which was approximately 1500 km in length, was produced by the release of convective instability due to synoptic-scale, warm-air advection at middle levels and dynamical processes related to the curvature of the flow (vorticity advection) within a migrating shortwave aloft.

By virtue of their elevation, the Rocky Mountains and Mexican Plateau produce a north–south-oriented potential temperature maximum that extends into the middle troposphere. As a synoptic shortwave disturbance moved eastward from Baja California on 8 March 1992, this air with high potential temperature underwent subsidence and differential horizontal ad-

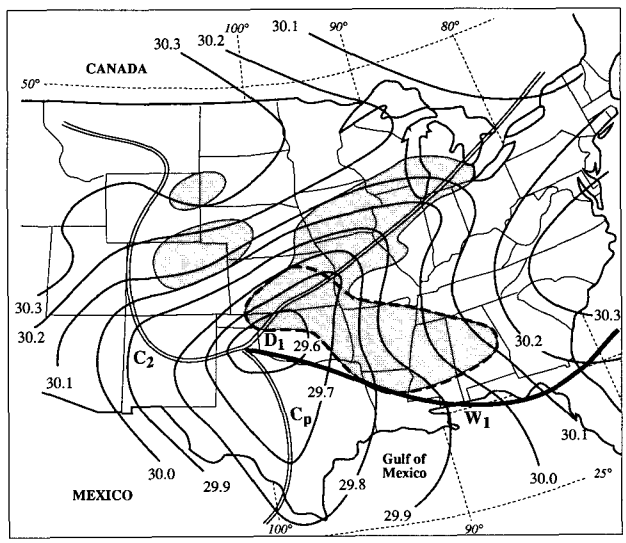

FIG. 22. Sea level pressure analysis for 0100 UTC 18 February 1926 (isobars are labeled in inches of mercury); C_p was analyzed as a cold front, W_1 as a warm front, C_2 as a secondary cold front, and D_1 as the center of lowest pressure. The rainband of interest is outlined by a heavy dashed line and other precipitation areas are shaded (adapted from Rossby and Weightman 1926).

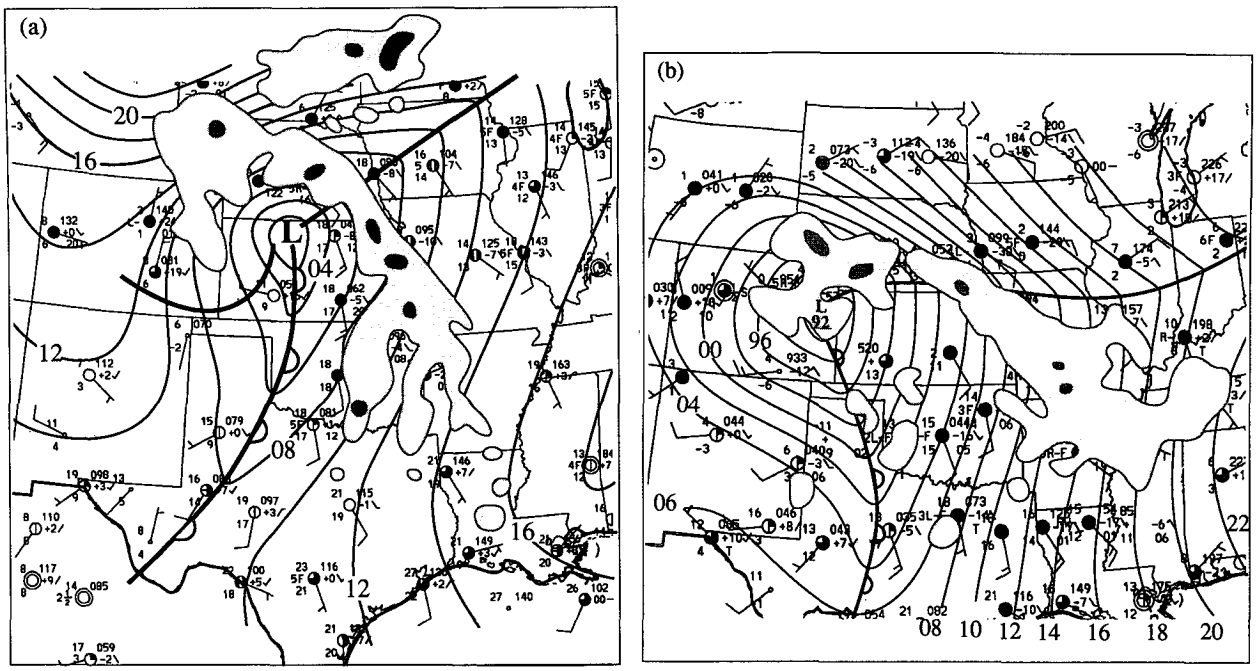

FIG. 23. (a) Sea level pressure analysis for 1200 UTC 8 October 1993 with the 1135 UTC 8 October NWS radar summary overlaid. Solid lines are isobars (mb, contoured every 2 mb); temperatures and dewpoints are given in degrees Celsius. Heavy solid line indicates the position of the arctic front east of the low pressure center and west of the low pressure center. Scalloped line indicates the position of the drytrough. (b) As for (a) but for 1200 UTC 12 November 1993.

vection. This established a low-level maximum of potential temperature near the surface that reduced the surface pressure. Continued warming and subsidence in the trough axis accelerated the low-level flow to the east of the trough axis, resulting in strong southerly flow east of the surface trough. The southerly flow advected extremely moist air, which originated over the Gulf of Mexico, as far north as southern Nebraska. The isolated region of maximum wind speed within this general southerly flow ahead of the trough (namely, the low-level jet) was particularly effective in transporting this moisture. Further, the horizontal deformation field associated with the deepening, subsidence-induced surface trough concentrated the significant background moisture gradient into a sharp horizontal moisture discontinuity. In this paper, we have termed this the drytrough, not only because it shared the characteristics of both a lee trough and a dryline, but also because these two features are, in many instances, including the case described here, one and the same.

As a result of the vertical wind shear characteristic of baroclinic waves, the region of warm air over the mountains at middle levels on 8 March 1992 was advected east more quickly at higher levels than at lower levels. This provided both a statically stable lid, which inhibited convection over a large area, and a downstream temperature gradient aloft. The temperature gradient, associated with the warm-air advection at middle levels, produced a predominantly northwesterly thermal wind, that isolated the low-level jet in the vertical.

A shallow warm-frontal circulation developed east of the drytrough in response to frontogenetic confluence acting on the meager gradient in the surface potential temperature east of the drytrough. This circulation forced moist air upward into the middle troposphere in a sloping zone that created a broad, elevated region of convective instability. This instability was eventually released in a narrow band, aligned along the warm edge of the warm-air advection at middle levels, to produce the pre-drytrough rainband.

As the cyclonic system developed and moved east of the leeward region of the Rockies, the region of warm air at middle levels was eliminated by adiabatic cooling from synoptic-scale ascent east of the axis of the upper-level trough and by being subsumed by the advection patterns associated with the developing wave.

Thus, the generation of the synoptic-scale structure, thermodynamics, and dynamics necessary for the production of the pre-drytrough rainband were all the result of the passage of a baroclinic wave over the high terrain and the manner in which the atmosphere adjusted to the differential horizontal advection of a deep pool of warm air that originally resided over the elevated terrain. Although some modifications to storm structure will always result from baroclinic flow over

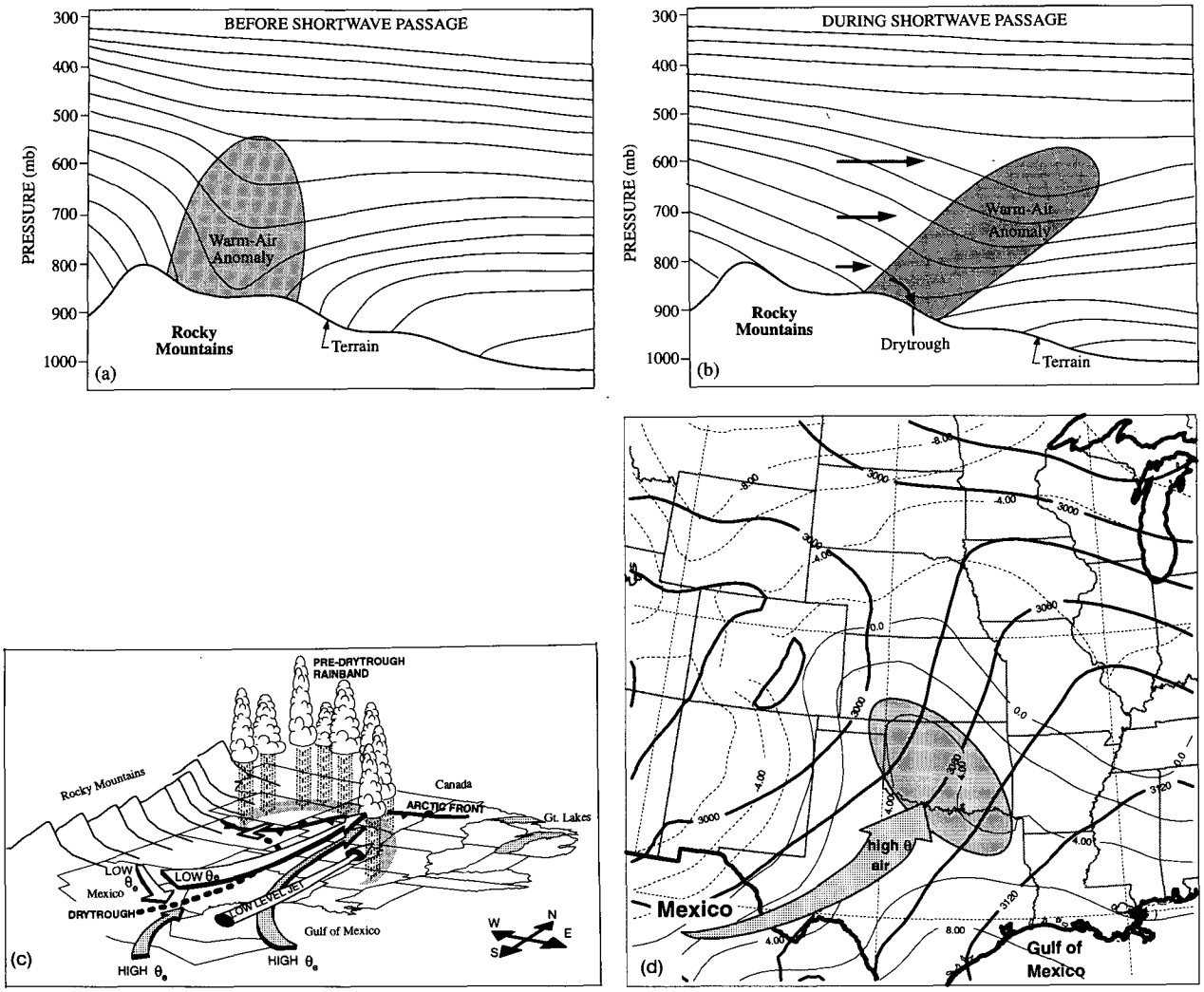

FIG. 24. (a) Schematic west–east cross section of the potential temperature field over the southern Rockies and southern plains of the United States before the passage of an upper short wave. Solid lines are isentropes and the warm-air anomaly is shaded. (b) Schematic west–east cross section of potential temperature during or after the passage of an upper-level shortwave over the Rocky Mountains. Solid arrows represent vertical shear of the baroclinic wave. The warm-air anomaly is shaded and tilts eastward with height. (c) Schematic of the circulation about the drytrough (dotted line) showing how it sets up the convectively unstable environment necessary for the formation of the pre-drytrough rainband. The low-level, confluent wind flow is indicated by arrows in northern Mexico, and the creation of the elevated, sloping region of convective instability is shown by the longer arrows to the north. (d) Schematic showing the origin of the warm-air anomaly at 700 mb. Heavy solid lines are geopotential height (m, contoured every 30 m), and lighter solid and dashed lines are isotherms (°C, contoured every 2°C). The tongue of warmest air is in dark shading, with its origin indicated by the shaded arrow marked "high θ air."

topography, the exact nature of the resulting structure, particularly its vigor, will depend on the temperature contrast between the warm air that resides over the Rockies and the Mexican Plateau and the air to the east of these features. In the present case, the drytrough, which provided the horizontal (LLJ) and vertical circulations necessary to create the required thermodynamic conditions for the formation of the pre-drytrough rainband, was the hydrostatic reflection of the warm-air anomaly at the surface, which was produced by subsidence off the high terrain of air with relatively high potential temperature. The warm potential temperature pool at middle levels, which had the characteristics of the elevated mixed layer described by Carlson et al. (1983), was located east of the drytrough as a result of the vertical shear in the baroclinic wave. Downstream of the axis of the warmest air at middle levels was a region of differential warm-air advection that, along with the advancing shortwave aloft, provided the lifting mechanism required to release the convective instability that gave rise to the pre-drytrough rainband. The thermal gradient characterizing the region of warm-air advection was oriented in such a way as to force a predominantly

northwesterly thermal wind, thus isolating the LLJ in the vertical.

Interestingly, in a paper that introduced the Norwegian cyclone model to the United States, Rossby and Weightman (1926) analyzed a cyclone similar to that described in this paper. This cyclone also contained a large rainband, similar to the one we have termed a pre-drytrough rainband. Figure 22 is a surface analysis from Rossby and Weightman, with the rainband of interest marked. They suggested that this rainband was produced by lifting at a warm front (labeled W_1 in Fig. 22). However, this warm front does not lie within a pressure trough and there is no significant wind shift across it. There is, however, a trough in central Texas across which there is a sharp wind shift. The wind speeds at Abilene, Texas, and Roswell, New Mexico (not shown), were extremely strong, similar to those observed west of the drytrough in the case described in this paper.

With reference to the rainband, Rossby and Weightman noted its unusual convective nature and stated that: "These thunderstorms cannot have their origin in surface convection." In fact, based on kite measurements, they concluded that the convection was generated at a height above 2000 m. Therefore, we suggest that the trough in central Texas in Fig. 22 was a drytrough, and that the rainband stretching from Kansas southeastward to Mississippi was a result of the release of convective instability triggered by the same processes as those that produced the pre-drytrough rainband described in this paper.

Two recent examples of surface cyclones with precipitation distributions remarkably similar to that described in this paper are shown in Fig. 23. In both cases, there is a convective rainband located well east of the surface trough that is clearly a drytrough.

These examples suggest that the various nonclassical features associated with winter cyclones east of the Rockies, which we have illustrated in some detail in this paper, are common. This is no doubt because the essential ingredient required for their development is the passage of a synoptic-scale baroclinic wave across the Rockies and Mexican Plateau.

8. Summary and conclusions

From about 1500 UTC 8 March until 1000 UTC 9 March 1992, a midlevel, convective precipitation event of modest intensity spread precipitation over parts of Oklahoma, Kansas, Nebraska, Colorado, Missouri, and Arkansas. This precipitation, which became banded at about 1800 UTC, formed within a large cyclonic development that was only beginning to organize during the lifetime of the rainband.

The synoptic-scale cyclonic structure within which the rainband formed was modified by its interaction with the high terrain of the Rockies and Mexican Plateau, resulting in the presence of a dryline and lee trough (or drytrough), a low-level jet, and a deep pool of warm air at middle levels. All of these features formed in response to westerly baroclinic flow across the Rockies and Mexican Plateau. A schematic cross section of the atmosphere, before passage of the short wave over the mountains, is shown in Fig. 24a. The drytrough was produced by a warm-air anomaly at the surface, which itself was produced by subsidence (Fig. 24b). The drytrough had a shallow, warm frontal–like, vertical circulation associated with it that advected high-θ_e boundary layer air into the middle troposphere where it created an elevated region of convective instability (Fig. 24c). The low-level jet, which formed in response to the strengthening of the pressure perturbation produced by the drytrough, assisted in advecting moisture ahead of the drytrough as far north as southern Nebraska (Fig. 24c). The warm-air advection at middle levels, which provided the synoptic-scale lifting necessary to release the instability and to form the pre-drytrough rainband, was located immediately downstream of a warm-air anomaly that was advected off the high terrain (Figs. 24b,d).

The types of nonclassical structures and precipitation features described in this paper are common in winter cyclonic storms in the central United States. This is because the essential ingredient for their development is the passage of a synoptic-scale short wave over the Rockies and Mexican Plateau.

Acknowledgments. We thank all the participants of STORM-FEST for their help in organizing the field project and collecting data. This research was supported by Grant ATM-9106235 from the Atmospheric Research Division of the National Science Foundation.

REFERENCES

Anthes, R. A., and T. T. Warner, 1978: Development of hydrodynamic models suitable for air pollution and other meso-meteorological studies. *Mon. Wea. Rev.*, **106,** 1045–1078.

——, E.-Y. Hsie, and Y.-H. Kuo, 1987: Description of the Penn State/NCAR Mesoscale Model Version 4 (MM4). NCAR Technical Note NCAR/TN-282+STR, 66 pp.

Benjamin, S. G., and T. N. Carlson, 1986: Some effects of surface heating and topography on the regional severe storm environment. Part I: Three-dimensional simulations. *Mon. Wea. Rev.*, **114,** 307–329.

Bennetts, D. A., and B. J. Hoskins, 1979: Conditional symmetric instability—A possible explanation for frontal rainbands. *Quart. J. Roy. Meteor. Soc.*, **105,** 945–962.

Bjerknes, J., and H. Solberg, 1922: Life cycle of cyclones and the polar front theory of atmospheric circulation. *Geofys. Publ.*, **12,** 1–61.

Blackadar, A. K., 1979: High resolution models of the planetary boundary layer. *Advances in Environmental Science and Engineering,* **1,** No. 1, Pffafflin and Zeigler, Eds., Gordon and Breach Sci. Pub., New York, 50–85.

Bonner, W. D., 1968: Climatology of the low-level jet. *Mon. Wea. Rev.*, **96,** 833–850.

Browning, K. A., M. E. Hardman, T. W. Harrold, and C. W. Pardoe, 1973: The structure of rainbands within a midlatitude depression. *Quart. J. Roy. Meteor. Soc.*, **99,** 215–231.

——, and G. A. Monk, 1982: A simple model for the synoptic analysis of cold fronts. *Quart. J. Roy. Meteor. Soc.*, **108,** 435–452.

Carlson, T. N., 1961: Lee side frontogenesis in the Rocky Mountains. *Mon. Wea. Rev.*, **89,** 163–172.

——, and F. H. Ludlam, 1968: Conditions for the occurrence of severe local storms. *Tellus,* **20,** 203–226.

——, S. G. Benjamin, and G. S. Forbes, 1983: Elevated mixed layers in the regional severe storm environment: Conceptual model and case studies. *Mon. Wea. Rev.*, **111,** 1453–1473.

Djuric, D., and M. S. Damiani Jr., 1980: On the formation of the low-level jet over Texas. *Mon. Wea. Rev.*, **108,** 1854–1865.

——, and D. S. Ladwig, 1983: Southerly low-level jet in the winter cyclones of the southwestern Great Plains. *Mon. Wea. Rev.*, **111,** 2275–2281.

Fujita, T., 1958: The structure and movement of a dry front. *Bull. Amer. Meteor. Soc.*, **39,** 574–582.

Gaza, R. S., and L. F. Bosart, 1985: The Kansas City severe weather event of 4 June 1979. *Mon. Wea. Rev.*, **113,** 1300–1320.

Grell, G., 1993: Prognostic evaluation of assumptions used by cumulus parameterizations. *Mon. Wea. Rev.*, **121,** 764–787.

Harrold, T. W., 1973: Mechanisms influencing the distribution of precipitation within baroclinic disturbances. *Quart. J. Roy. Meteor. Soc.*, **99,** 232–251.

Hobbs, P. V., 1978: Organization and structure of clouds and precipitation on the mesoscale and microscale in cyclonic storms. *Rev. Geophys. and Space Phys.*, **16,** 741–755.

——, T. J. Matejka, P. H. Herzegh, J. D. Locatelli, and R. A. Houze Jr., 1980: The mesoscale and microscale structure and organization of clouds and precipitation in mid-latitude cyclones. I: A case study of a cold front. *J. Atmos. Sci.*, **37,** 568–596.

——, J. D. Locatelli, and J. E. Martin, 1990: Cold fronts aloft and the forecasting of precipitation and severe weather east of the Rocky Mountains. *Wea. Forecasting,* **5,** 613–626.

Holzman, B., 1936: Synoptic determination and forecasting significance of cold fronts. *Mon. Wea. Rev.*, **64,** 400–413.

Keyser, D., and T. N. Carlson, 1984: Transverse ageostrophic circulations associated with elevated mixed layers. *Mon. Wea. Rev.*, **112,** 2465–2478.

Lichtblau, S., 1936: Upper cold fronts in North America. *Mon. Wea. Rev.*, **64,** 414–425.

Lloyd, J. R., 1942: The development and trajectories of tornadoes. *Mon. Wea. Rev.*, **70,** 65–75.

Locatelli, J. D., J. M. Sienkiewicz, and P. V. Hobbs, 1989: Organization and structure of clouds and precipitation on the Mid-Atlantic coast of the United States. Part I: Synoptic evolution of a frontal system from the Rockies to the Atlantic coast. *J. Atmos. Sci.*, **46,** 1327–1348.

——, J. E. Martin, and P. V. Hobbs, 1994: A wide cold-frontal rainband and its relationship to frontal topography. *Quart. J. Roy. Meteor. Soc.*, **120,** 259–275.

——, ——, and ——, 1995: Development and propagation of precipitation cores on cold fronts. *Atmos. Res.*, **32,** in press.

Martin, J. E., J. D. Locatelli, and P. V. Hobbs, 1990: Organization and structure of clouds and precipitation on the mid-Atlantic coast of the United States. Part III: The evolution of a middle-tropospheric cold front. *Mon. Wea. Rev.*, **118,** 195–217.

——, ——, and ——, 1992: Organization and structure of clouds and precipitation on the mid-Atlantic coast of the United States. Part V: The role of an upper-level front in the generation of a rainband. *J. Atmos. Sci.*, **49,** 1293–1303.

Matejka, T. J., R. A. Houze Jr., and P. V. Hobbs, 1980: Microphysics and dynamics of clouds associated with mesoscale rainbands in extratropical cyclones. *Quart. J. Roy. Meteor. Soc.*, **106,** 29–56.

McCarthy, J., and S. E. Koch, 1982: The evolution of an Oklahoma dryline. Part I: A meso- and subsynoptic-scale analysis. *J. Atmos. Sci.*, **39,** 225–236.

McGuire, E. L., 1960: The vertical structure of three drylines as revealed by aircraft traverses. *First AMS Conference on Severe Local Storms,* St. Louis, MO, Amer. Meteor. Soc., 1–11.

Means, L. L., 1952: On thunderstorm forecasting in the central United States. *Mon. Wea. Rev.*, **80,** 165–189.

Palmen, E., and C. W. Newton, 1969: *Atmospheric Circulation Systems.* Academic Press, New York, 603 pp.

Parsons, D. B., M. A. Shapiro, R. M. Hardesty, R. J. Zamora, and J. M. Intrieri, 1991: The finescale structure of a west Texas dryline. *Mon. Wea. Rev.*, **119,** 1242–1258.

Rhea, J. O., 1966: A study of thunderstorm formation along dry lines. *J. Appl. Meteor.*, **5,** 59–63.

Rossby, C.-G., and R. H. Weightman, 1926: Application of the polar-front theory to a series of American weather maps. *Mon. Wea. Rev.*, **54,** 485–496.

Schaefer, J. T., 1974: The life cycle of the dryline. *J. Appl. Meteor.*, **13,** 444–449.

——, 1986: The dryline. *Mesoscale Meteorology and Forecasting,* P. Ray, Ed., Amer. Meteor. Soc., 549–570.

Shapiro, M. A., and D. A. Keyser, 1990: Fronts, jet streams and the tropopause. *Extratropical Cyclones: The Erik Palmen Memorial Volume,* C. Newton and E. Holopainen, Eds., Amer. Meteor. Soc., 167–189.

Sienkiewicz, J. M., J. D. Locatelli, P. V. Hobbs, and B. Geerts, 1989: Organization and structure of clouds and precipitation on the mid-Atlantic coast of the United States. Part II: The mesoscale and microscale structure of some frontal rainbands. *J. Atmos. Sci.*, **46,** 1349–1364.

Steenburgh, W. J., and C. F. Mass, 1994: The structure and evolution of a simulated Rocky Mountain lee trough. *Mon. Wea. Rev.*, **122,** 2740–2761.

Zhang, D.-L., and R. A. Anthes, 1982: A high-resolution model of the planetary boundary layer: Sensitivity tests and comparisons with SESAME-79 data. *J. Appl. Meteor.*, **21,** 1594–1609.